Helmholtz-Zentrum Geesthacht
Zentrum für Material- und Küstenforschung

Final Draft
of the original manuscript:

Tilstone, G.H.; Peters, S.W.M.; van der Woerd, H.J.; Eleveld, M.A.; Ruddick, K.; Schoenfeld, W.; Krasemann, H.; Martinez-Vicente, V.; Blondeau-Patissier, D.; Roettgers, R.; Soerensen, K.; Joergensen, P.V.; Shutler, J.D.:

Variability in specific-absorption properties and their use in a semi-analytical ocean colour algorithm for MERIS in North Sea and Western English Channel Coastal Waters

In: Remote Sensing of Environment (2012) Elsevier

DOI: 10.1016/j.rse.2011.11.019

Variability in specific-absorption properties and their use in a semi-analytical Ocean Colour algorithm for MERIS in North Sea and Western English Channel Coastal Waters.

Gavin H. Tilstone[1*], Steef W. M. Peters[2], Hendrik Jan van der Woerd[2], Marieke A. Eleveld[2], Kevin Ruddick[3], Wolfgang Schönfeld[4], Hajo Krasemann[4], Victor Martinez-Vicente[1], David Blondeau-Patissier[1,5#], Rüdiger Röttgers[4], Kai Sørensen[6], Peter V. Jørgensen[7†], Jamie Shutler[1].

[1]*Plymouth Marine Laboratory (PML), Prospect Place, West Hoe, Plymouth, PL1 3DH, UK.*

[2]*Institute for Environmental Studies (IVM), Faculty of Earth and Life Sciences, Vrije Universiteit, De Boelelaan 1087, 1081 HV Amsterdam, THE NETHERLANDS*

[3]*Management Unit of the North Sea Mathematical Models (MUMM), Royal Belgian Institute for Natural Sciences (RBINS), 100 Gulledelle, B-1200 Brussels, BELGIUM*

[4]*Institute for Coastal Research Forschungszentrum Geesthacht (HZG), Max-Planck-Institute, D-21502 Geestacht, GERMANY*

[5]*Aquatic Remote Sensing Group, CSIRO Land & Water, GPO Box 1666, Canberra ACT 2601, AUSTRALIA*. [#]Present address.

[6]*Norwegian Institute for Water Research (NIVA), Gaustadalléen 21, NO 0349, NORWAY*

[7]*Danish Meteorological Institute (DMI), Copenhagen, DENMARK*

[†]Current address: *Ministry of Food, Agriculture and Fisheries, Landbrug og Fiskeri, Direktoratet for FødevareErhverv, Nyropsgade 30, 1780 København V, DENMARK.*

*Corresponding author Email: ghti@pml.ac.uk, Tel: ++ 44 1752 633100, FAX: ++ 44 1752 633101.

KEY WORDS: Case 2 waters, Inherent Optical Properties, North Sea, Ocean Colour Remote Sensing, Phytoplankton, Western English Channel.

Abstract

Coastal areas of the North Sea are commercially important for fishing and tourism, and are subject to the increasingly adverse effects of harmful algal blooms, eutrophication and climate change. Monitoring phytoplankton in these areas using Ocean Colour Remote Sensing is hampered by the high spatial and temporal variation in absorption and scattering properties. In this paper we demonstrate a clustering method based on specific-absorption properties that give accurate water quality products from the Medium Resolution Imaging Spectrometer (MERIS). A total of 468 measurements of Chlorophyll a (Chla), Total Suspended Material (TSM), specific- (sIOP) and inherent optical properties (IOP) were measured in the North Sea between April 1999 and September 2004. Chla varied from 0.2 to 35 mg m^{-3}, TSM from 0.2 to 75 g m^{-3} and absorption properties of coloured dissolved organic material at 442 nm ($a_{CDOM}(442)$) was 0.02 to 0.26 m^{-1}. The variation in absorption properties of phytoplankton (a_{ph}) and non-algal particles (a_{NAP}) were an order of magnitude greater than that for a_{ph} normalized to Chla (a_{ph}*) and a_{NAP} normalized to TSM (a_{NAP}*). Hierarchical cluster analysis on a_{ph}*, a_{NAP}* and a_{CDOM} reduced this large data set to three groups of high a_{NAP}*-a_{CDOM}, low a_{ph}* situated close to the coast, medium values further offshore and low a_{NAP}*-a_{CDOM}, high a_{ph}* in open ocean and Dutch coastal waters. The median sIOP of each cluster were used to parameterize a semi-analytical algorithm to retrieve concentrations of Chla, TSM and $a_{CDOM}(442)$ from MERIS data. A further 60 measurements of normalized water leaving radiance (nL_w), Chla, TSM, $a_{CDOM}(442)$ and $a_{NAP}(442)$ collected between 2003 and 2006 were used to assess the accuracy of the satellite products. The regionalized MERIS algorithm showed improved performance in Chla and $a_{CDOM}(442)$ estimates with relative

percentage differences of 29 and 8% compared to 34 and 134% for standard MERIS Chla and $a_{dg}(442)$ products, and similar retrieval for TSM at concentrations >1 gm^{-3}.

1. Introduction

Information on marine environmental parameters, such as Chlorophyll a (Chla), is becoming increasingly important as it describes key parameters for monitoring climate change, water quality and the effects of pollution in the marine environment (Justic et al. 1996; Yunev et al. 2005). Large scale spatial and temporal information on these parameters can be obtained by means of satellite remote sensing which can aid our understanding of biogeochemical cycles (Bousquet et al. 2006; Mohr and Forsberg 2002). Long term time series of satellite ocean colour have shown an increase in Chla by 20% in sub-tropical regions over the past two decades but a decrease in Chla in oligotrophic gyres (Antoine et al. 2005), which are related to multi-decadal changes in ocean physics (Martinez et al. 2009). Primary production has decreased in the northern hemisphere (Tilstone et al. 2009) and at low latitudes, which is tightly coupled to increases in temperature and a reduction in nutrients as the result of enhanced stratification events (Behrenfeld et al. 2006). It is however, more difficult to accurately determine Chla from satellite in coastal regions due to their optical complexity (IOCCG 2000). Despite their relatively small area, accounting for just 7% of the world ocean's surface, coastal zones play an important part in the global carbon cycle and in buffering human impacts on marine systems. They support 10-15% of the world ocean net annual productivity and may be responsible for > 40 % of the annual carbon sequestration (Muller-Karger et al. 2005). Coastal areas of the North Sea are commercially important for fishing and tourism, yet are subject to the increasingly adverse effects of harmful algal blooms (Aanesen et al. 1998; Maestrini and Graneli 1991), eutrophication (Lancelot et al. 1987) and climate change (Reid et al. 2001; Stige et al. 2006). There is therefore an obvious

need to develop accurate Chla algorithms in coastal regions to monitor these environmental changes.

Understanding the optical variability in the marine environment is important since it aids the development of satellite algorithms, especially in optically complex coastal areas. In most oceanic waters, which occupy approximately 60 % of the global ocean (Lee and Hu 2006), light absorption by phytoplankton dominates and is modified by the 'pigment package effect' (Bricaud et al. 2004a), which is a function of cell size, species type and pigment concentration within the cell. Low pigment concentrations are predominantly associated with small phytoplankton cells, and high pigment concentrations with large cells (Yentsch and Phinney 1989). In these waters, the absorption coefficient of coloured dissolved organic material (a_{CDOM}) is coupled with variations in phytoplankton biomass and can be modified by microbial and photochemical degradation (Del Vecchio and Blough 2002; Hedges et al. 1997). In coastal regions, where the presence of Coloured Dissolved Organic Material (CDOM) and Total Suspended Material (TSM) also modify the light field (IOCCG 2000), accurate estimation of Chla from satellite is more difficult. CDOM and TSM originating from riverine run-off and re-suspension of bottom sediment, are highly variable and on a global basis, the combined absorption of coloured dissolved organic and detrital material (a_{dg}) contribute up to 40% of the non-water absorption at 440nm in the subtropical gyres and 60% at high latitudes (Siegel et al. 2005b). To facilitate algorithm development, Morel and Prieur (1977) classified optical water types into either Case 1 waters, where the optical properties are governed by phytoplankton, or Case 2 waters which are additionally affected by absorption properties of coloured dissolved organic material

(a_{CDOM}) and TSM that do not co-vary with phytoplankton. A plethora of algorithms were developed to detect Chla in Case 1 waters and the most successful was an empirical, band switching ratio, which is accurate to 25% for Chla concentrations up to 35 mg m^{-3}. This algorithm was adopted by NASA as the standard Sea-viewing Wide Field of view Sensor (SeaWiFS) open ocean algorithm (O'Reilly et al. 1998). It often fails in Case 2 waters because the optical signature of CDOM or TSM can mask phytoplankton absorption at 442nm (Sathyendranath et al. 2001). Prieur and Sathyendranath (1981) suggested seven water types based on the relative importance of the absorption coefficients of phytoplankton (a_{ph}), non-algal particles or detrital material (a_{NAP}) and a_{CDOM} to the total absorption in the water column. From these a number of algorithms were developed to retrieve inherent optical properties (IOP) and biogeochemical parameters from optically complex Case 2 waters (Carder et al. 1999; Doerffer and Schiller 2007; Lee et al. 2002; Maritorena et al. 2002), which also provide additional parameters other than Chla (IOCCG 2006). A number of semi-analytical approaches have been used in which water constituent concentrations are derived from the IOP, through a knowledge of the specific-inherent optical properties (sIOP) i.e. the IOP normalised to its biogeochemical concentration (van der Woerd and Pasterkamp 2008; Lee et al. 2002; Smyth et al. 2006). These methods have advantages over conventional band ratio algorithms in that multiple ocean properties can be retrieved simultaneously from a single water-leaving radiance spectrum. The availability of data from satellite sensors such as Moderate Resolution Imaging Spectroradiometer (MODIS-Aqua) and Medium Resolution Imaging Spectrometer (MERIS), which have more spectral bands, a higher spatial resolution than SeaWiFS and novel atmospheric correction models, have also facilitated the development

of a new range of satellite products for coastal waters. The current diversity of IOP models, however, exhibit large differences in performance when retrieving total absorption, backscatter or decomposing these into individual optically active components (IOCCG 2006), primarily because they are trained on a limited IOP data set (Claustre and Maritorena 2003; Cota et al. 2003; Sathyendranath et al. 2001). This is also compounded by the fact that with inverse modeling techniques, several combinations of IOP can lead to the same reflectance spectrum (Defoin-Platel and Chami 2007).

There have been few studies of variations in IOP and sIOP in the optically complex coastal waters of the North Atlantic and the implementation of this data in ocean colour algorithms for case 2 waters. North Sea and English Channel coastal areas have high absorption and scattering properties (Hommersom et al. 2009), and can switch seasonally between case 1 and 2 water types (Groom et al. 2009). The variability in a_{CDOM} in these areas is strongly linked to seasonal cycles of riverine run off and water column mixing (Garver and Siegel 1997). The most comprehensive analysis of the optical properties of European waters, which included the North Sea, was conducted by Babin et al. (2003a; 2003b). From over 350 stations, they found that there were significant departures from the general trend between $a_{ph}(\lambda)$ and Chla reported for oceanic waters due to a different pigment composition and cell size under the influence of varying a_{CDOM} and a_{NAP}, and that that low light scattering at 555nm was principally due to minerals with a low clay and silt content that occur along the European shelf. Due to its optical complexity, the North Sea has been a site for satellite algorithm development: A Chla atlas of the region was published using NASA-Coastal Zone Color Scanner (CZCS) global algorithm as a qualitative proof of concept (Holligan et al. 1989). More recently, a

neural network algorithm was developed, firstly calibrated on North Sea data and then globally, to give standard global coastal products of Chla, TSM and a_{dg} from MERIS data (Doerffer and Schiller 2007). Directional water leaving radiance is input to the algorithm and it outputs Chla, TSM and a_{dg} based on the conversion of scattering and absorption coefficients using non linear multiple inversion solutions and regional conversion factors to give concentrations. Regionally tuned algorithms for the North Sea have also been developed to retrieve Chla (Hokedal et al. 2005; Peters et al. 2005) and TSM (van der Woerd and Pasterkamp 2004) based on either radiative transfer solutions using the numerical model HYDROLIGHT to estimate concentrations of optically active substances from modeled reflectance spectra or regionally tuned spectral shapes and slopes input to empirical solutions.

In this paper we addressed the following questions: What is the temporal and spatial variation in absorption and specific-absorption properties in the North Sea and Western English Channel? What are the principal absorption and specific-absorption properties in this area? Can trends in specific-absorption properties alone be used to develop accurate ocean colour regional algorithms? The variation in specific-absorption properties in the North Sea and Western English Channel is analysed using hierarchical clustering to characterise the principal optical types. Representative sIOP groups are then used, in conjunction with a semi-analytical model HYDROPT, to retrieve water quality parameters Chla, TSM and CDOM. To demonstrate the benefits of this method, the products from this regionally tuned model are compared to standard MERIS Case 2 water products.

2. Methods

2.1. Study area characteristics and sampling regime

Seven research institutes measured the bio-optical properties and associated biogeochemical concentrations of 468 stations on 21 cruises from 1998 to 2003 in the North Sea, Western English Channel (WEC) and Celtic Sea (Table 1a, Figure 1a). A further 61 stations were sampled on a further 15 cruises to measure Chla, TSM, $a_{CDOM}(\lambda)$ and normalized water leaving radiance ($nL_w(\lambda)$) by four institutes in the North and Celtic Seas from March 2003 to September 2006 (Table 1b, Figure 1b). This second set of measurements was used to perform an accuracy assessment of satellite products. On all cruises, surface water samples were collected using 10l Niskin bottles.

Fig. 1 Near Here.

Table 1 Near Here.

2.2. Measurement of biogeochemical parameters

2.2.1. Chlorophyll-a

Danish Meteorological Institute (DMI), Institute for Coastal Research (HZG), Mathematical modelling unit for the North Sea (MUMM), Norwegian Institute for Water Research (NIVA) and Plymouth Marine Laboratory (PML) measured Chla by High Pressure Liquid Chromatography (HPLC). Between 0.25 and 2 L of seawater were filtered onto 25mm, 0.7 µm GF/F filters and phytoplankton pigments were extracted in methanol containing an internal standard apo-carotenoate (Sigma-Aldrich Company Ltd.). Chla extraction was either by freezing at -30°C or using an ultrasonic probe following the methods outlined in Sørensen et al. (2007). Pigments were identified using retention time and spectral match using Photo Diode Array (Jeffrey et al. 1997) and Chla

concentration was calculated using response factors generated from calibration using a Chla standard (DHI Water and Environment, Denmark). The Institute for Environmental Studies (IVM) extracted Chla using 80% ethanol at 75°C and concentrations were determined spectrophotometrically, by measuring the extinction coefficients at 665 and 750 nm before and after acidification with 0.20 ml HCl (0.4 mol l^{-1}) per 20 ml of filtrate.

2.2.2. Total Suspended Material (TSM)

For measurements made by HZG, MUMM, NIVA and PML, between 0.5 and 3 L of seawater was filtered onto 47 mm, 0.7 μm GF/F filters in triplicate, which were ashed at 450°C and then washed for 5 mins in 0.5 L of MilliQ to remove friable fractions that can be dislodged during filtration. The filters were then dried in a hot air oven at 75°C for one hour, pre-weighed and stored in desiccators (Van der Linde 1998). Seawater samples were filtered in triplicate and the filters and filter rim were washed three times with 0.05 L MilliQ to remove residual salt. Blank filters were also washed with MilliQ to quantify any potential error due to incomplete drying. The filters were then dried at 75°C for 24 hrs and weighed on microbalances (detection limit 10 μg). TSM concentrations were determined from the difference between blank and sample filters and the volume of seawater filtered. Samples analysed by DMI were measured in the same way but were dried at 65°C for one hour. The IVM samples were pre-ashed at 550°C and then dried at 105°C.

2.3. Measurement of Inherent Optical Properties.

2.3.1. Phytoplankton ($a_{ph}(\lambda)$) and non-algal particle ($a_{NAP}(\lambda)$) absorption coefficients.

HZG, NIVA and PML filtered between 0.25 and 2 L of seawater onto 25mm, 0.7 μm. The absorbance of the material captured on the filter was then measured from 350-750 nm at a 1 nm bandwidth using dual beam spectrophotometers retro-fitted with spectralon coated integrating spheres, following the transmission-reflectance method of Tassan and Ferrari (1995). Measurements were made of total particulate absorption ($a_{part}(\lambda)$) and $a_{NAP}(\lambda)$ retained on GF/F filters before and after pigment extraction with NaClO 1% active chloride. The pathlength amplification correction of Tassan and Ferrari (1998) was used and $a_{ph}(\lambda)$ was derived from the difference between $a_{part}(\lambda)$ and $a_{NAP}(\lambda)$. IVM and DMI measured $a_{part}(\lambda)$ in transmission mode only with an Ocean Optics FC UV200-2 and a Shimadzu UV-2401 spectrophotometer, respectively. The $a_{NAP}(\lambda)$ was also measured in transmission mode after pigment extraction in 80% ethanol at 75ºC following the methods of Kishino et al. (1985). Chlorophyll specific absorption coefficients ($a_{ph}^*(\lambda)$) and suspended particulate matter specific absorption coefficients ($a_{NAP}^*(\lambda)$) were calculated by dividing $a_{ph}(\lambda)$ and $a_{NAP}(\lambda)$ by their respective Chla and TSM concentrations.

2.3.2. CDOM absorption coefficients ($a_{CDOM}(\lambda)$).

All laboratories filtered replicate seawater samples through 0.2 μm Whatman Nuclepore membrane filters into acid cleaned glassware. The first two 0.25 L of the filtered seawater were discarded and $a_{CDOM}(\lambda)$ of the third sample was determined in a 10 cm quartz cuvette from 350 to 750 nm relative to a bi-distilled MilliQ reference blank. The samples were analysed immediately on board using the spectrophotometers except for samples collected off East Anglia, UK, which were spiked with 0.5 ml solution of 10 gl^{-1} of NaN_3

per 100 ml of seawater (Ferrari et al. 1996) and stored in a refrigerator for less than 10 days until analysis to prevent sample degradation (Mitchell et al. 2000). The $a_{CDOM}(\lambda)$ was calculated from the optical density of the sample and the cuvette path length.

2.3.3. Particulate scattering coefficients (b_p).

Particulate scattering coefficient (b_p) was calculated at nine wavelengths (412, 440, 488, 510, 555, 630, 650, 676 and 715 nm) from dual WetLabs ac9 absorption and attenuation profiles measured at stations in the North Sea and WEC by HZG, NIVA & PML. Measurements were made at a resolution of 5 nm and with an accuracy of 0.005 m^{-1} following WetLabs protocols (WetLabs 2007). Water calibrations were performed to account for the attenuation and absorption of pure water to monitor any drift in the sensors. Temperature and salinity correction was performed following (Pegau et al. 1997)(1997). and methods 1 and 3 were used for scattering correction (Zaneveld et al. 1994). The data were binned to 1 m values, discarding peaks in the top 5 m due to bubbles.

2.4. Characterization of specific-Inherent Optical Properties in the North Sea.

To characterize the stations by sIOP type, Primer-E v6.1.5 Cluster Analysis (Clarke and Gorley 2006) was applied to 316 sIOP data. The Ward method of hierarchical agglomerative clustering on squared Euclidian distance was employed (Ward 1963), in which the Euclidian distance between two stations is the sum of the squared differences between the values of the clustering variables. A SIMPROF test was applied to each node of the dendogram using a significance level of 5% (Clarke and Gorley 2006), which

highlights branches with no remaining structure so that the main clusters can be identified quantitatively.

2.5. Measurement of Apparent Optical Properties.

Measurements were performed by HZG and MUMM with three TriOS-RAMSES hyperspectral spectro-radiometers, two measuring radiance and one measuring downwelling irradiance as in Ruddick et al. (2005). The instruments were mounted on a steel frame, so that zenith angles of the sea- and sky viewing radiance sensors were 40°. The frame was fixed to the bow of the ship, facing forward to minimize ship shadow and reflection (Hooker and Morel 2003). The ship was maneuvered on station to point the radiance sensors at a relative azimuth angle of 135° away from the sun, to reduce sun glint and bidirectional reflectance effects. IVM used a Photo Research 650 hand held spectro-radiometer. Measurements were from 350 to 950 nm every 10 s for 10 min, coincident with global positioning system (GPS) data. The spectro-radiometers were calibrated before and after the cruise consistent with SeaWiFS protocols (Mueller et al. 2003). Water-leaving reflectance (ρ_w) was calculated from simultaneous above-water measurements of downwelling irradiance, E_d^{0+}; total upwelling radiance (i.e., from the water and from the air-sea interface) at a zenith angle of 40°, L_{sea}^{0+}; and sky radiance, L_{sky}^{0+}, in the direction of the region of sky that reflects into the sea viewing sensor, by:

$$\rho_w(\lambda) = \pi \frac{L_{sea}^{0+}(\lambda) - \rho_{sky} L_{sky}^{0+}(\lambda)}{E_d^{0+}(\lambda)} \qquad (1)$$

where ρ_{sky} is the air-water interface reflection coefficient for radiance which is equal to the Fresnel reflection coefficient in the case of a flat sea surface and is assumed to be

0.02 for clear skies (Ruddick et al. 2005), which was the case for satellite 'match-ups'. Residual skylight was removed using baseline correction following Mobley (1999). nL_w was calculated as follows:

$$nL_w(\lambda) = \frac{\rho_w(\lambda)}{\pi} \times f_0(\lambda) \text{ (in mW cm}^{-2}\ \mu\text{m}^{-1}\ \text{sr}^{-1}\text{)} \quad (2)$$

where $f_0(\lambda)$ is the mean solar flux above the earth's atmosphere.

2.5. Variation between laboratories in the measurement of biogeochemical parameters, apparent and inherent optical properties.

To quantify measurement differences between laboratories, an inter-calibration experiment was performed between HZG, NIVA and PML from 9 to 14 June 2002 (Tilstone et al. 2004a). All laboratories used the same measurement protocols (Tilstone et al. 2004b). Surface water was collected by *RV Squila* from three stations in the WEC close to the Plymouth coast. All variables were measured in triplicate by each laboratory. For HPLC Chla, there was no significant difference between laboratories ($F_{2,26} = 0.70$, $P = 0.51$) and the maximum difference in Chla concentration between laboratories was 9%. There was also no significant difference between laboratories for a_{ph} at MERIS bands ($F_{2,80} = 0.43$, $P = 0.84$). The maximum difference in $a_{ph}(442)$ between laboratories was 14% and 10% at $a_{ph}(680)$. There was no significant difference between laboratories for the measurement of TSM ($F_{2,53} = 0.30$, $P = 0.74$) and the maximum difference between laboratories was 20%. Similarly, there was no significant difference between laboratories for a_{CDOM} at MERIS bands ($F_{2,80} = 1.34$, $P = 0.27$), which were within 20%. During the inter-calibration exercise, each institute measured *in situ* parameters in triplicate; the estimated uncertainty in each of the parameters (average percentage standard deviation)

was 22% for Chla, 15% for TSM, 4% for $a_{CDOM}(442)$ and 10% for $a_{ph}(442)$ and $a_{NAP}(442)$. For nL_w, the sky, nadir and sea surface radiometers were calibrated in the laboratory using a NIST traceable lamp and the difference in radiometers was <5% between laboratories. The differences between laboratories for all parameters were smaller than the variations in these parameters in the field and we therefore expect there to be no bias due to systematic errors in measurements in UK, Belgium, German and Norwegian waters.

2.6. Accuracy assessment of Remote sensing algorithms

In addition to, and independent of, the initial 468 measurements described in section 2.2, a further 61 measurements of Chla, 51 measurements of nL_w, 51 measurements of TSM and 14 measurements of $a_{CDOM}(442)$ & $a_{NAP}(442)$ were made between 2003 and 2006 (Table 1b, Figure 1b) for an accuracy assessment of MERIS algorithms.

MERIS reduced resolution (1.2 x 1.2 km) level 2 data, 2nd reprocessing (R2005) using the 'bright pixel' atmospheric correction for Case 2 waters (Moore et al. 1999), were downloaded from the European Space Agency. The standard Case 2 MERIS products from the neural network (NN) algorithm (Doerffer and Schiller 2007) Chla algal pigment 2 (AP2), $a_{dg}(442)$ and TSM, were extracted using Beam v4.8. The following MERIS quality flags were used to eliminate erroneous data: cloud flag over ocean (CLOUD), land (LAND), no glint correction applied – accuracy uncertain (HIGH_GLINT), reflectance corrected for medium glint – accuracy maybe degraded (MEDIUM_GLINT), highly absorbing aerosols (AODB), low sun angle (LOW_SUN), low confidence flag for water leaving or surface reflectance (PCD1_13) and reflectance

out of range (PCD_15). The MERIS L2 products were extracted from a 3 x 3 pixel box, within ±0.5 hrs of MERIS overpasses.

The semi-analytical algorithm HYDROPT (Van der Woerd and Pasterkamp 2008) was also used with the same R2005 MERIS data. HYDROPT comprises a forward model based on the HYDROLIGHT radiative transfer model (Mobley 1994) and an inverse model based on least-square fitting of the MERIS measured to modelled reflectance (Garver and Siegel 1997; Maritorena et al. 2002). The forward model generates a lookup table (LUT) of ρ_w as a function of the absorption (a) and scattering (b) properties and their constituent Chla, TSM and a_{CDOM}, as follows:

$$\rho_w = f\left(a, b, \theta_s, \theta_v, \varphi_s, \varphi_v, Fresnel\ \ coefficient_{water-sky}\right)$$

Equation 1

where f is a function, θ_s is the solar zenith angle, θ_v is the viewing zenith angle, φ_s is the solar azimuth angle, φ_v is the viewing azimuth angle and the Fresnel coefficient is the factor required for the water-sky interface. The algorithm predicts remote sensing reflectance spectrum from a and b through knowledge of the sIOP for a particular region as follows:

$$a(\lambda) = a_w(\lambda) + a_{ph}^*(\lambda) \times Chla + a_{NAP}^*(\lambda) \times TSM + a_{CDOM}^*(\lambda) \times a_{CDOM}(440)$$

Equation 2

$$b(\lambda) = b_w(\lambda) + b_p^*(\lambda) \times TSM$$

Equation 3

where a_w and b_w are the absorption and scattering coefficients of pure water. HYDROPT was parameterized with median sIOP values (a_{CDOM}*, a_{ph}*, a_{NAP}*, and b_p*) from the main cluster groups identified using the methods described in Section 2.4. The HYDROPT

algorithm was run using MERIS data in bands 1 to 9, to estimate concentrations of Chla, TSM and $a_{CDOM}(442)$. The scattering phase functions in the forward radiative transfer model were a uniform scattering function for pure water and the 'San Diego harbor' scattering phase function for TSM (Petzold 1972). The algorithm retrieves the concentrations from each sIOP type, by minimizing the chi square (X^2) difference between observed MERIS and modeled reflectance spectra stored in the LUT (Mobley et al. 2005) at consecutive MERIS bands; 413, 442, 490, 510, 560, 617, 665, 681 and 708, as follows:

$$\chi^2 = \sum_{i=1}^{i=m} \left[\frac{(R_{RS_{i+1}MERIS} - R_{iMERIS}) - (R_{RS_{i+1}Modelled} - R_{iModelled})}{\sigma} \right]^2$$

Equation 4

where i is the band number, m is the band number minus 1 and σ is the estimated standard error between bands based on Rast et al. (1999). The NN and HYDROPT use the same LUT. The only difference between them is in the bio-optical modeling and the use of different sIOP datasets to retrieve the LUT values to match the MERIS and modelled reflectance. For HYDROPT, each sIOP type input is evaluated on a pixel by pixel basis, and the sIOP type with the smallest X^2 difference is selected. The sIOP data used in HYDROPT are not fixed and can be calibrated quickly using an 'external' data set, whereas the MERIS NN algorithm requires extensive 'internal' calibration.

To evaluate algorithm performance we used the mean (M), standard deviation (S), and root-mean square (RMS) of the difference error (D) between measured and satellite products at each station as described in Campbell et al. (2002). The geometric mean and one-sigma range of the inverse transformed ratio between satellite and measured values are given by M (F_{med}), M-S (F_{min}), M+S (F_{max}) and were used as algorithm performance

indices. The relative (RPD) and absolute percentage differences (APD) were calculated following Antoine et al. (2008). We also used one way analysis of variance (ANOVA) to test for significant differences between *in situ* and satellite products. Kolomogrov - Smirnov with Lilliefors tests were used to check whether the distribution of *in situ* and satellite products were normal. The ANOVA results are given as $F_{1,108} = x$, $P = y$ where F is the mean square to mean square error ratio, the sub-script numbers denote the degrees of freedom and P is the ANOVA critical significance value.

3. Results

3.1. Variation in biogeochemical concentrations, inherent and specific-inherent optical properties in the North Sea.

Chla and $a_{ph}(442)$ were significantly higher along the Dutch Coast (Chla $F_{8, 413} = 6.25$, $P < 0.0001$; $a_{ph}(442)$ $F_{8, 338} = 9.71$, $P < 0.0001$) followed by the German Bight, West Jutland and Belgium coasts and lowest in the NW North Sea and WEC (Figure 2a, b). $a_{ph}^*(442)$ was significantly higher in the Celtic Sea ($F_{8, 402} = 6.26$, $P < 0.0001$) and lowest on the Dutch coast and the SE North Sea (Figure 2c). $a_{CDOM}(442)$ varied by 100 times and was highest in the Skagerrak, German Bight and NW North Sea and was significantly lower in the Celtic, NE North Sea and WEC ($F_{8, 407} = 42.96$, $P < 0.0001$; Figure 2d). TSM varied by over 350 times and was highest along the German Bight, Belgium and Dutch coasts and low in the WEC, Celtic Sea, SE, NW North Sea and Skagerrak (Figure 2e). $a_{NAP}(442)$ was higher along Dutch, Belgium, German and UK East Anglia coasts (Figure 2f). $a_{NAP}^*(442)$ was significantly higher along the West Jutland coast ($F_{7, 330} = 2.58$, $P = 0.013$) and lowest in the SE North Sea and WEC (Figure

2g). There were fewer b_p and b_p* data available (n=172). From these, b_p had higher values in German and Dutch coastal regions and significantly lower values in the SE North Sea and WEC ($F_{5, 176} = 9.40$, $P < 0.001$; data not shown). By comparison, b_p*(560) was significantly higher in the NW North Sea ($F_{5, 176} = 24.91$, $P < 0.001$) and the lowest values occurred in the SE North Sea and UK East Anglia coast (Figure 2h).

Fig. 2 Near Here.

Figure 3a shows the relationship between $a_{ph}(442)$ and Chla for spring and summer in the North Sea and surrounding environs. We found that $a_{ph}(442) = 0.0543<Chl>^{0.675}$, which explained 67 % of the variability in $a_{ph}(442)$, and is slightly lower than the power law commonly used for case 1 and 2 waters by Bricaud et al. (2004), which is also plotted in Figure 3a. For the regression between TSM and $a_{NAP}(442)$ (Figure 3b) we found that $a_{NAP}(442) = 0.0242$ TSM ($r^2 = 0.60$), which is slightly lower than the relationship reported by Babin et al. ((2003c), which we also plot in Figure 3b.

Fig. 3 Near Here.

Using the ternary absorption budget proposed by Prieur and Sathyendranath (1981), we characterise the optical water types based on absorption properties (i.e. a_{ph}, a_{NAP}, a_{CDOM}, a_{ph}-a_{CDOM}, a_{NAP}-a_{CDOM}, a_{ph}-a_{NAP}-a_{CDOM}) and map them over the ten geographic regions sampled (Figure 4a, b). Some clear patterns in the absorption properties emerge: The Skagerrak was dominated by $a_{CDOM}(442)$ with a couple of stations during the spring bloom dominated by $a_{ph}(442)$ (Figure 4a, b). The German Bight, Dutch, Belgium and UK coasts were either co-dominated by a_{ph}, a_{NAP} and $a_{CDOM}(442)$ or by a_{ph} and $a_{CDOM}(442)$. The SE North Sea, WEC and parts of the Celtic Sea were also co-dominated by a_{ph} and $a_{CDOM}(442)$. Only three stations in the Celtic Sea, SE North Sea and

Dutch Coast were dominated by $a_{ph}(442)$ alone. a_{NAP} and $a_{CDOM}(442)$ co-dominated in the inner German Bight and some stations on the Belgium coast (Figure 4b). There were no stations where a_{ph} and a_{NAP} co-dominated (Figure 4b).

Fig. 4 Near Here.

In Figure 5 we depict the ternary plot given in Figure 4a for different seasons, to illustrate the temporal shift in absorption parameters. Of the ten geographic regions listed (Table 1a, Figure 1a), six were sampled in April and May (spring; Figure 5a), eight in June and July (summer; Figure 5b), five in August and September (autumn; Figure 5c) and two from October to March (winter; Figure 5d). From spring to winter in the German Bight $a_{CDOM}(442)$ generally dominated but the relative contributions of a_{ph} and a_{NAP} shifted with season so that in spring more stations were dominated by $a_{ph}(442)$, whereas in autumn and winter the stations sampled had a higher proportion of $a_{NAP}(442)$. From April to September the WEC stations were either high $a_{ph}(442)$ and low $a_{CDOM}(442)$ or low a_{ph} and high a_{CDOM} (Figure 5a, b, c) reflecting the influence of the Atlantic inflow from the Celtic Sea or the freshwater outflow from River Tamar. By winter, the WEC samples were dominated by $a_{CDOM}(442)$ alone (Figure 5d). The Dutch coast samples tended to have higher $a_{ph}(442)$ in April and May (Figure 5a) but higher $a_{CDOM}(442)$ in August and September (Figure 5c). The Skagerak samples remained high a_{CDOM}, low a_{ph} and a_{NAP} from April to September (Figure 5a, b, c).

Fig. 5 Near Here.

To compare the distribution of IOP with sIOP we employed cluster analysis on coincident measurements of $a_{CDOM}(442)$, $a_{ph}^*(442)$ and $a_{NAP}^*(442)$. The analysis segregated three principal clusters (Figure 5c). The largest (Cluster 2, n = 161) grouped

stations with low a_{ph}*, high a_{NAP}* and a_{CDOM}, which also had high b_p* (median values a_{ph}*(442) 0.029 ± 0.012 mg m^{-2}, a_{NAP}*(442) 0.041 ± 0.023 g m^{-2}, a_{CDOM}(442) 0.367 ± 0.287 m^{-1}, b_p* 0.36 ± 0.31 m^2 g TSM^{-1}; Figure 6) from the Belgium, Danish and German coasts. The second largest (Cluster 3, n = 137) grouped stations with medium a_{ph}*, a_{NAP}* and a_{CDOM} which had lower b_p* (median a_{ph}*(442) 0.041 ± 0.022 mg m^{-2}, a_{NAP}*(442) 0.018 ± 0.013 g m^{-2}, a_{CDOM}(442) 0.227 ± 0.164 m^{-1}, b_p* 0.28 ± 0.20 m^2 g TSM^{-1}; Figure 6) from the Southern Bight between the Belgium and UK coasts, NE North Sea, WEC and Skagerrak. The smallest cluster (Cluster 1, n = 18) grouped stations with high a_{ph}*, low a_{NAP}* and a_{CDOM} from the WEC, Celtic and SE North Seas (median a_{ph}*(442) 0.047 ± 0.147 mg m^{-2}, a_{NAP}*(442) 0.012 ± 0.013 g m^{-2}, a_{CDOM}(442) 0.062 ± 0.073 m^{-1}, too few b_p* data, default value used; Figure 6).

Fig. 6 Near Here.

To assess the influence of river discharge in the coastal zone on the absorption and specific-absorption properties we plot the relationships between a_{CDOM}(442) and a_{NAP}(442) and salinity (Figure 7a, b) as a function of the optical types from the ternary absorption budget given in Figure 4b. We also plot a_{CDOM}(442) and a_{NAP}*(442) against salinity as a function of the main sIOP groups from the cluster analysis (Figure 7c, d). For a_{CDOM}(442) and salinity we observed two main regressions; one for a_{CDOM} and a_{ph}-a_{CDOM} type waters, where $a_{CDOM}(442) = -0.020*\text{Salinity} - 0.91$ ($r^2 = 0.24$, $P = 0.0002$; dashed line in Figure 7a) which corresponds to the relationship observed for sIOP Cluster 3 ($a_{CDOM}(442) = -0.015*\text{Salinity} - 0.72$, $r^2 = 0.35$, $P < 0.0001$; dashed line in Figure 7c). The other a_{CDOM}(442)-salinity regression was for a_{NAP}-a_{CDOM} and a_{NAP}-a_{ph}-a_{CDOM} type waters where $a_{CDOM}(442) = -0.066*\text{Salinity} + 2.35$ ($r^2 = 0.93$, $P<0.0001$; solid line in

Figure 7a) which corresponds to the relationship observed for sIOP Cluster 2 where $a_{CDOM}(442) = -0.058*\text{Salinity} + 2.12$, ($r^2 = 0.70$; solid line in Figure 7c). For $a_{NAP}(442)$ and salinity there was one significant regression for a_{NAP}-a_{CDOM} and a_{NAP}-a_{ph}-a_{CDOM} type waters, where $a_{NAP}(442) = -0.042*\text{Salinity} + 1.58$ ($r^2 = 0.49$, $P<0.0001$; solid line in Figure 7b), illustrating that low $a_{NAP}(442)$ is associated with higher salinity stations influenced by Atlantic water and high $a_{NAP}(442)$ is associated with stations in coastal waters influenced by river runoff. The other regression plotted in Figure 7b is for the a_{CDOM} and a_{ph}-a_{CDOM} type waters but was not significant since $a_{NAP}(442)$ was consistently low with varying salinity. By comparison, the regression between $a_{NAP}*(442)$ and salinity explained a lower percentage of variance and Cluster 2 and 3 had similar slopes (Cluster 3 $a_{NAP}*(442) = -0.0011*\text{Salinity} + 0.053$, $r^2 = 0.12$; Cluster 2 $a_{NAP}*(442) = -0.0013*\text{Salinity} + 0.08$, $r^2 = 0.05$, Figure 7d), illustrating a weaker link between $a_{NAP}*(442)$ and river discharge. There was no significant regression between $a_{ph}(442)$ and $a_{ph}*(442)$ and salinity for any of the Cluster groups (data not shown).

Fig. 7 Near Here.

3.3. Accuracy assessment of MERIS derived products.

The median values in sIOP at MERIS bands 1-9 from the three groups characterized by the cluster analysis (Figure 6) were used to parameterize the semi-analytical algorithm HYDROPT. There were few $b_p*(555)$ data available for Cluster 1 to be statistically representative of this group, so the default reference value was used. We then used the 61 *in situ* match-up points for Chla, 51 for nL_w, 51 for TSM, and 14 for $a_{CDOM}(442)$ and $a_{NAP}(442)$ to assess the accuracy of both standard MERIS ocean colour and the newly parameterized HYDROPT algorithm (Figure 8, 9). The majority of the stations were from

the Belgium coast, the others were from the German Bight, NW North Sea and Celtic Sea (Table 1b, Figure 1b).

Firstly we assessed the 2nd reprocessing of MERIS nL_w against *in situ* nL_w to evaluate the accuracy of the satellite radiometers and atmospheric correction (Figure 8). The range in *in situ* $nL_w(442)$ at the validation stations was 0.2 to 0.54 mW cm^{-2} μm^{-1} sr^{-1}. Generally the RMS, bias, RPD and APD decreased and F_{med}, F_{min}, F_{max} increased from $nL_w(412)$ to $nL_w(560)$ (Table 2), indicating that MERIS is more accurate in the North Sea at 560nm than at 412, 443 and 490nm. The APD for $nL_w(665)$ was similar to that in the blue, though the RPD and RMS were lower (Table 2). The regression slope was closer to 1 for MERIS $nL_w(442)$ compared to $nL_w(560)$ and $nL_w(665)$, but the offset was higher (Figure 8).

Fig. 8 Near Here.

Table 2 near here.

For MERIS Chla algorithms the log_{10}-RMS was 0.26, indicating agreement with *in situ* values within a factor of 2 (Table 2). The range in Chla at the validation stations was 0.26 to 27.57 mg m^{-3} and the geometric means (F_{med}, F_{min}, F_{max}) were close to 1 for both AP2 and HYDROPT, indicating a high level of accuracy over the range tested. The random error (S) and bias (M and RPD) of both algorithms was low ($S<0.3$, $M<0.1$), though MERIS AP2 had a slightly higher APD since it tended to under-estimate Chla at values <5 mg m^{-3} (Table 2, Figure 9a). HYDROPT Chla exhibited a smaller bias indicated by the lower RMS (Table 2, Figure 9b). As a consequence, in satellite images from 22 April 2003, MERIS AP2 gave higher Chla values during the spring bloom in the

Celtic Sea, SE, NW North Sea, Skagerrak and WEC compared to HYDROPT, but lower values in continental European coastal areas (Figure 10a, b).

Fig. 9 Near Here.

In situ TSM at the match-up stations varied between 1.01 to 95.22 g m^{-3} and at least 65% of the stations had TSM >3.0 g m^{-3}. We found that for the North Sea, MERIS and HYDROPT TSM had a similar log_{10}-RMS, but MERIS had a lower S. The F_{med} was closer to 1 for HYDROPT, but the F_{max} was closer to 1 for MERIS (Table 2, Figure 9c, d), which resulted in a regression slope closer to 1 for HYDROPT compared to MERIS TSM. For HYDROPT RPD and APD were higher due to a higher scatter at lower TSM values (Figure 9d). This resulted in a lower estimate in HYDROPT TSM values in the Celtic Sea, WEC and in Norwegian waters in April 2003, compared to MERIS TSM, but a higher estimate in the Southern Bight, Belgium, Dutch and UK coastal waters (Figure 10c, d). TSM concentrations were similar for both algorithms along the German Bight.

The range in $a_{CDOM}(442)$ and $a_{dg}(442)$ at the validation stations was 0.01 to 0.673 m^{-1} and 0.027 to 1.71 m^{-1}, respectively. Compared to MERIS $a_{dg}(442)$ algorithm, the RMS values were lower for HYDROPT $a_{CDOM}(442)$ and indicate an agreement with *in situ* values of ~1.5, whereas the difference for MERIS $a_{dg}(442)$ was a factor of ~3 (Table 2). The random error (S), bias (M and RPD), APD and intercept for the HYDROPT algorithm were also lower, F_{med} and F_{min} values and slope were closer to 1, which also shows a closer agreement between *in situ* and HYDROPT $a_{CDOM}(442)$ compared with MERIS $a_{dg}(442)$ (Table 2, Figure 9e, f). There was a slight tendency for HYDROPT to over-estimate $a_{CDOM}(442)$ at high values when Cluster 2 was implemented (Figure 9f). For MERIS $a_{dg}(442)$ there was a consistent under-estimation when values were <0.06 m^{-}

[1]. The spatial pattern in MERIS $a_{dg}(442)$ and HYDROPT $a_{CDOM}(442)$ satellite maps of 22 April 2003 was similar, but the values in some areas were very different (Figure 10e, f). For example, in the Celtic Sea, SE North Sea and West Jutland Belgium and Dutch coasts, MERIS $a_{dg}(442)$ was an order of magnitude higher than HYDROPT $a_{CDOM}(442)$.

Fig. 10 Near Here.

4. Discussion

4.1. Variation in inherent and specific-inherent optical properties of the North Sea.

A comparison of the mean absorption properties of the North Sea from our data with historic studies is given in Table 3. There is high similarity in our $a_{ph}(442)$ and $a_{ph}^*(442)$ with those from previous studies indicating that the 468 data we collected is representative of the variability in IOP sIOP of the North Sea. Our mean $a_{ph}(442)$ for the North Sea was 0.16 m^{-1} and similar to that of Babin et al. (2003b) and Vantrepotte et al. (2007). Our mean $a_{ph}^*(442)$ was 0.044 m^2 mg $Chla^{-1}$ and similar to the values given in Staehr et al. (2004) and Tilstone et al. (2005). The $a_{CDOM}(442)$ values we report are also similar to those given for the North Sea (Astoreca et al. 2009), English Channel (Vantrepotte et al. 2007) and other UK coastal areas (Foden et al. 2008), but lower than some data sets for the Baltic Sea and Skagerrak. When only data from coastal regions were included in our analysis, $a_{CDOM}(442)$ was significantly lower on the East Anglia, UK and Belgium coasts (mean~0.2 m^{-1}; $F_{5, 346} = 2.32$, $P = 0.043$), whereas it was higher and similar along the German Bight (mean~0.42 m^{-1}), Skagerrak (~0.38 m^{-1}), Dutch coast (~0.34 m^{-1}) and West Jutland (~0.31 m^{-1}). We found our $a_{NAP}(442)$ values, to be slightly higher than those values previously reported for the North Sea, English Channel and Irish Sea, 50% less than those values reported for other European estuarine and coastal waters

(Table 3), but within a similar range to those given in Babin et al. (2003) and Ferrari et al. (2003). The higher $a_{NAP}(442)$ is due to high values along the Dutch coast, resulting from a high organic content of the TSM in the Wadden Sea (Hommersom et al. 2009), probably resulting from high Chla in these waters and agricultural runoff to the coast. For $a_{NAP}^*(442)$, few values have been reported for the North Sea (Table 3). We found that $a_{NAP}^*(442)$ was significantly higher on the West Jutland coast due to comparatively low TSM (Figure 2g), indicating high organic detritus in these waters, possibly due to the soil type and agricultural runoff on the West coast of Denmark as suggested by Stedmon et al. (2000). A detailed analysis of b_p for this area has already been conducted by Babin et al. (2003a), who showed that light scattering at 555nm was principally due to minerals with a low clay and silt content that occur along the European shelf. Babin et al. (2003a) reported mean $b_p^*(559)$ of 0.54 m^2g^{-1} for coastal waters of the North Sea. Our mean value of 0.44 m^2g^{-1} for the North Sea and WEC is slightly lower than this due to the inclusion of more stations in coastal waters and possibly due to the difference in pore size of filters used. In our study, the same protocols were used by each laboratory and inter-calibration exercises showed that there was no significant bias in measurements between laboratories. The 95% confidence interval of $a_{ph}^*(442)$, $a_{NAP}^*(442)$, $b_p^*(560)$ and $a_{CDOM}(442)$ were low and did not produce significant deviations from the mean, indicating that the error associated with this data set was low. In addition, we confirmed that our IOP and sIOP value were typical of the North Sea by comparing with previous literature values (Table 3).

The power law commonly used for a_{ph} as a function of Chla is $a_{ph}(440) = 0.0654(TChla)^{0.728}$ (Bricaud et al. 2004b). Using the 392 Chla data points from this study,

we used the Bricaud et al. (Bricaud et al. 2004b) relationship and our model to calculate $a_{ph}(440)$ and found a significant difference between models ($F_{1, 569} = 17.76$, $P < 0.0001$). The Bricaud et al. (2004b) data was predominantly collected in case 1 waters with some stations in coastal waters, whereas our data was mostly from case 2 waters, where the difference in the under water light regime due to higher TSM and a_{CDOM} may modify the a_{ph}-Chla relationship. For $a_{NAP}(442)$ and TSM we found that $a_{NAP}(442) = 0.0242*TSM$ ($r^2 = 0.60$). Similarly Bowers and Mitchelson-Jacob (1996) reported that $a_{NAP}(443) = 0.0235*TSM$. The relationship reported by Babin et al. (2003c) was slightly higher $a_{NAP}(443) = 0.031*TSM$, probably because their data included more open ocean stations and they used a smaller filter pore size 0.2µm. For the 343 TSM data collected during this study we used each model to re-calculate $a_{NAP}(443)$ and found no difference between our model and those of Bowers and Mitchelson-Jacob (1996) and Babin et al. (2003c) ($F_{2, 1028} = 2.41$, $P = 0.090$), suggesting that any of these relationships could be used with the same relative accuracy to derive TSM from satellite.

The ternary plot of absorption (Figure 4a), indicates that the North Sea is principally dominated by $a_{CDOM}(442)$ or co-dominated by $a_{CDOM}(442)$ and $a_{ph}(442)$. Less than 1% of the stations were dominated by $a_{NAP}(442)$ which represent waters with a high organic TSM content that absorb light. However, $a_{NAP}(442)$ is a poor proxy for classifying inorganic sediments which have little capacity for absorbing light. Alternatively, Siegel et al. (2005a) used the single scatter approximation and the absorption of phytoplankton and CDOM as a ternary plot to assess the contribution of these to the diffuse attenuation coefficient, $k_d(\lambda)$. On a global basis, they found that the contribution of $b_{bp}(\lambda)$ to $k_d(\lambda)$ was <10%, Chla contributed 40% and a_{dg} accounted for

50% of the variability. Scattering and backscattering properties are as important to ocean colour as absorption properties, but in the absence of a comprehensive $b_p(\lambda)$ and $b_{bp}(\lambda)$ data sets, we employed cluster analysis on specific-absorption properties to assess the relatedness in these properties between stations. This approach is also complementary with the optical water types original identified by Prieur and Sathyendranath (1981). From the principal clusters identified, there were broadly three main groups which radiated in bands from the coast. Cluster 1 had low $a_{NAP}^*(442)$, $a_{CDOM}(442)$ and high $a_{ph}^*(442)$, occupying open ocean stations. Cluster 2 with low $a_{ph}^*(442)$, high $a_{NAP}^*(442)$ and $a_{CDOM}(442)$ occurred close to the coast. Cluster 3 occupied stations between the coast and open ocean and in the Skagerak with medium $a_{ph}^*(442)$, $a_{NAP}^*(442)$ and $a_{CDOM}(442)$ (Figure 4c). The Norwegian coast is influenced by a deep inflow of Atlantic water and a surface outflow of Baltic water, which results in high a_{CDOM} along the southern Norwegian (Høkdal et al. 2005) and Danish coasts (Stedmon et al. 2000). The east-west separation in sIOP characterised by Cluster 2 and 3 therefore seems to be by stations influenced by riverine run-off from continental Europe and UK coasts (Cluster 2) and those influenced by Baltic Sea and shelf areas (Cluster 3). Though the European Continental coastal margin is influenced by high a_{CDOM} from the fresh water outflow of the Elbe, Rhine and Scheldt rivers (Warnock et al. 1999), our analysis suggests that these stations are also associated by high $a_{NAP}^*(442)$, which differentiates stations further offshore with lower $a_{NAP}^*(442)$ values. There were similarities between the cluster analysis and the ternary plot of absorption properties; Cluster 3 had a similar geographic distribution to a_{ph}-a_{CDOM} (Figure 4b, c). Cluster 1 corresponded to the location of a_{ph} and

a_{ph}-a_{CDOM} dominated stations and Cluster 2 had a similar geographic distribution to a_{CDOM}-a_{NAP} type stations.

Temporally in spring and summer, coastal North Sea areas were dominated more by a_{ph} and a_{CDOM}. In autumn and winter there was a tendency for these regions to become more strongly influenced by a_{CDOM} and a_{NAP} due to the low phytoplankton biomass, increased riverine runoff and sediment resuspension. It has previously been observed that in winter, the entrance of warm, high saline water into the North Sea, through the Orkney-Shetland inflow in the north (off NE Scotland) and through the English Channel-Straits of Dover in the south, drives a cyclonic pattern of circulation which causes re-suspension of sediment over the shallow North Sea shelf (Reid et al. 1988). In the Southern Bight, high TSM concentrations also occur (>30 mg m^{-3}) due to the influence of the River Thames outflow and the re-suspension of sediment over the shallow shelf (<50m), which forms a characteristic sediment plume off the south east UK coast (van der Woerd and Pasterkamp 2004). We only had data available in winter from the WEC and German Bight. The WEC switched between sIOP type Cluster 1 from June to September to Cluster 3 from October to April. Similarly in the eastern English Channel, Vantrepotte et al. (2007) found that a_{CDOM} dominates the optical signal during winter, and from spring to summer phytoplankton and a_{CDOM} co-dominate. By contrast, in the German Bight Cluster 3 was the predominant sIOP type from March to August and Cluster 2 occurred from October to February (data not shown).

A negative correlation between blue spectral bands of a_{CDOM} and salinity is commonly reported in European Coastal waters (!!! INVALID CITATION !!!). The regressions between $a_{CDOM}(442)$ and salinity highlighted two principal optical types; one

co-dominated by a_{NAP}-a_{ph}-a_{CDOM} which occupied stations close to the coast; the other co-dominated by a_{ph}-a_{CDOM} which dominated stations further offshore. The regression between $a_{NAP}(442)$ and salinity and sIOP Cluster types suggest three distinct optical waters in the North Sea: 1.) Waters dominated by a_{CDOM} and a_{ph} typical of stations in the Skagerak and transitional coastal-offshore zone with a salinity range of 15 to 35 characterised by low a_{CDOM}-salinity slope (sIOP Cluster type 3); waters dominated by a_{CDOM} and a_{NAP} mainly comprised of continental European and UK coastal stations also with a high range in salinity but with a higher a_{CDOM}-salinity slope (sIOP type Cluster 2); and waters dominated by a_{ph} typical of stations in the Celtic and SE North Seas with a salinity range of 30.5 to 35.5 (sIOP type Cluster 1). These optical water types are similar to those described by Aarup et al. (1996) and Hojerslev et al. (1996) based on the regression between a_{CDOM} and salinity alone, but the geographic regions differ slightly when Cluster analysis on sIOP data was used: (1.) North Sea water with high salinity and low CDOM, (similar to Cluster 1), (2.) Baltic Sea water with low salinity and intermediate to high CDOM (similar to Cluster 3 which also included coastal-offshore transition waters) and (3.) German Bight/Southern North Sea water with intermediate to high salinity and high CDOM (similar to Cluster 2 which shows a zonal band that links European coastal areas).

4.2. Accuracy assessment of regional sIOP MERIS algorithm

4.2.1. Normalized Water leaving radiance

This is the first study of the validation of MERIS 2nd reprocessed R2005 in highly turbid waters and therefore complementary to the validation of these MERIS data in case 1 waters (Antoine et al. 2008). Recent studies based on continuous *in situ* measurements

from towers or buoys have shown that MERIS over-estimates $nL_w(442)$ globally, by 44% (Maritorena et al. 2010) and at coastal sites in the Adriatic-Baltic by 39% (Zibordi et al. 2009; Zibordi et al. 2006b), in the Mediterranean by 36% (Antoine et al. 2008) and in the Skagerrak 40% (Sorensen et al. 2007). In North Sea coastal waters, we found the difference to be 64%. This may be attributed to errors in the standard aerosol model of optical thickness used in the atmospheric correction (Aznay and Santer 2009) or to failure in the correction in turbid waters or at cloud borders (Gomez-Chova et al. 2007) which will potentially be improved in the 3rd reprocessing MERIS data (Lerebourg and Bruniquel 2011). At least 65% of the stations in our validation data set had TSM >3.0 g m^{-3}, where atmospheric correction may start to fail (Esaias et al. 1998), which was evident for MERIS $nL_w(412)$, $nL_w(442)$ and $nL_w(490)$ (Figure 8, Table 2). The difference between *in situ* and MERIS nL_w improved at 560nm and the 665 nm (Table 2) and the RPD and APD for North Sea coastal areas were similar to those reported both globally (APD; 20% at 560 nm, 125% at 665 nm), in the Baltic and Adriatic (APD; 18% at 560 nm, 47% at 665 nm), the Mediterranean (RPD; 25% at 560 nm, 70% at 665 nm) and in the Skagerrak (RPD; 10% at 560 nm, 40% at 665 nm) (Antoine et al. 2008; Zibordi et al. 2006a).

4.2.2. Chlorophyll-a

By implementing median sIOP values at MERIS bands 1-9 from three the principal cluster analysis groups, we found that HYDROPT Chla was more accurate than MERIS AP2 and $\log_{10}$-RMS improved from 0.26 for MERIS AP2 to 0.17 for HYDROPT. The differences in Chla retrieval between the algorithms is likely to be due to the calibration data sets used. The AP2 algorithm is a NN calibrated on a global dataset, which included

a large IOP data set from North Sea coastal waters of the German Bight (Schiller and Doerffer 2005), where Chla, TSM and a_{CDOM} are high compared to other regions (Figure 2). In this version of HYDROPT, the calibration data set includes IOP from a wider variety of coastal waters, including the Skagerrak, NW North Sea and Celtic Sea, where Chla, TSM and a_{CDOM} are lower (Figure 2). The calibration dataset used for HYDROPT is therefore probably more representative of variations in IOP in North Sea coastal waters. Though the difference in RPD was only 5%, this represents a significant improvement for optically complex coastal waters where the retrieval accuracy of Chla can be 73-100% (Hooker and McClain, 2000; Moore et al. 2009). In addition, HYDROPT selects on a pixel by pixel basis the sIOP group that matches the modeled and MERIS reflectance spectra, so that any number of sIOP data sets can be input, as illustrated here. By comparison, the NN derives a_{ph} and b_p and through empirical bio-optical relationships, IOP are converted to Chla and TSM concentrations, but any modification to the NN requires extensive 'internal' calibration. Where MERIS AP2 tended to under-estimate Chla, the HYDROPT algorithm proved to have a greater accuracy over the range tested (Figure 7a, b) and especially at low Chla values where Cluster 1 and 3 were the predominant sIOP type (Figure 7b). For MERIS AP2, Chla = $26.21*a_{ph}(442)^{0.771}$, and for all data in this study Chla = $25.65*a_{ph}(442)^{0.979}$. For HYDROPT the relationships varied from Chla = $2.45*a_{ph}(442)^{0.289}$ for Cluster 1, Chla = $28.62*a_{ph}(442)^{0.925}$ for Cluster 2 and Chla = $20.81*a_{ph}(442)^{0.876}$ for Cluster 3, which accounts for the differences at the lower end of the Chla range tested when Cluster 1 and 3 sIOP types were implemented (Figure 7b). The original HYDROPT algorithm was reported to be accurate for Chla concentrations between 1 and 20 mg m^{-3}, with accuracy

decreasing when Chla <0.5 mg m^{-3}, when $a_{CDOM}(442)$ >1 m^{-1} or when TSM is >20 g m^{-3} (Van der Woerd and Pasterkamp 2008). The HYDROPT algorithm used in this study is a new variant of the model parameterized on a more comprehensive sIOP dataset for the North Sea, and has extended the range of Chla to ~30 mg m^{-3} and is accurate at high TSM and $a_{CDOM}(442)$ values. In addition, this new parameterization of the algorithm, has extended its accuracy to Case 1 waters to Chla <0.5 mg m^{-3}.

4.2.3. Total Suspended Matter

For TSM, $\log_{10}$-RSM was similar for both algorithms and they showed similar retrieval accuracy for values from 1-95 g m^{-3} TSM, though the regression slope for HYDROPT was closer to 1 than that for MERIS TSM. MERIS however showed better retrieval accuracy at TSM concentrations <1.0 g m^{-3}, which reduced the APD, RPD and S (Table 2). MERIS NN calibration for TSM is principally based on $b_p^*(560)$, whereas HYDROPT TSM is derived from $b_p^*(\lambda)$ and $a_{NAP}^*(\lambda)$ at all MERIS bands. An over-estimate in MERIS $nL_w(442)$ and under-estimate in MERIS $nL_w(560)$ and $nL_w(665)$ would result in lower $a_{NAP}(\lambda)$, which was the case when Cluster 1 and 3 sIOP types were implemented (Figure 7d). This resulted in the higher scatter for the HYDROPT TSM algorithm at low *in situ* TSM, which will probably be improved in the 3rd MERIS reprocessing data due to improvements in the atmospheric correction. $b_p^*(560)$ tends to increase as the water becomes more oceanic, or less coastal as scattering efficiency increases offshore, as a response to changes in particle size, type and shape (Babin et al. 2003a; Bowers and Binding 2006). The $b_p^*(560)$ values we used from Cluster 2 and 3 to parameterize HYDROPT (Figure 7) are comparable with values measured in the English Channel (Loisel et al. 2007; Martinez-Vicente et al. 2010), but higher than those reported

for the neighbouring Irish Sea (Bowers and Binding 2006). The number of spectra available for Cluster 1 was low (Figure 6), so we used the default reference b_p* from the original parameterization (Van der Woerd and Pasterkamp 2008), which according to Bowers and Binding (2006) could be too low. The median b_p*(560) values used for Clusters 1 were similar to that used for Cluster 3; as a result, HYDROPT under-estimated eight of the *in situ* TSM values that were between 1 and 9 g m^{-3}. If these values were removed from the data set, HYDROPT had a lower log_{10}-RMS and S (0.27, -0.07) compared to MERIS (0.32, -0.19) for TSM retrieval. To improve TSM retrieval at concentrations <1 g m^{-3}, more b_p* data are required to parameterise HYDROPT for the case 1 waters of the North and Celtic Seas.

4.2.1. Coloured dissolved organic matter

HYDROPT outputs a_{CDOM} whereas MERIS NN only outputs a_{dg} and cannot distinguish a_{CDOM} from a_{NAP}. HYDROPT a_{CDOM}(442) was consistently more accurate than MERIS a_{dg}, though the number of points available for validation was lower than for Chla and TSM validation. The over-estimate in MERIS nL_w(442) and the error in the MERIS a_{dg} probably occurs in the partitioning between a_{dg}, a_{ph} and b_p by the NN. The original version of HYDROPT was optimized for retrieving Chla in waters with a_{CDOM}(442) from 0.01 to 1.0 m^{-1}. This new version of the algorithm parameterized with three different sIOP groups can accurately retrieve Chla and a_{CDOM}(442) from 0.01 to 2.6 m^{-1}. The ability to distinguish a_{CDOM} from a_{NAP}, and to predict a_{CDOM} accurately is ultimately what is required for water quality monitoring in the coastal zone, to derive dissolved organic carbon (DOC) due to the tight coupling between DOC and a_{CDOM} in coastal waters (Keith et al. 2002). In this paper we have proven that this is possible for HYDROPT.

Improvements in the atmospheric correction procedure for MERIS due in 3rd reprocessing data are likely to improve the accuracy of both the standard MERIS a_{dg} and HYDROPT $a_{CDOM}(442)$.

We found that trends in specific-absorption properties alone can be used to develop accurate ocean colour regional algorithms for Chla and $a_{CDOM}(442)$ in both coastal and offshore waters. This approach was also accurate for retrieval of TSM >1 g m^{-3}, but for values <1 g m^{-3} a better characterization of b_p* properties in waters dominated by a_{ph}, is required. The 3rd reprocessing of MERIS data is likely to improve both the MERIS case 2 and HYDROPT algorithms due to the new vicarious adjustment of the marine reflectance and the new 'bright pixel' atmospheric correction model for AP2, TSM and a_{dg} products. It will be interesting to quantify how future changes in the next generation MERIS reprocessing will affect the accuracy of standard MERIS and HYDROPT products in coastal waters. This study demonstrates the benefits and future potential of HYDROPT products for monitoring coastal areas.

4.3. The benefits and limitations of the sIOP HYDROPT method.

For the HYDROPT algorithm, no pre-defined boundaries of the sIOP types characterized by the cluster analysis are necessary, since the algorithm chooses the sIOP based on the best match by minimizing the difference between observed and modeled reflectance spectra from HYDROLIGHT. The retrieval of biophysical variables from optical data can be problematic (Defoin-Platel and Chami 2007). With several combinations of biophysical variables resulting in similar remote sensing reflectance, it is important to limit the possible ranges of biophysical values. To accommodate this, Defoin-Platel and Chami (2007) suggested dividing the global problem-set into more

localized versions that better represent bio-optical conditions found in common environments. In this study we achieved this by using a forward model and by classifying the principal sIOP types over coastal and shelf seas using cluster analysis. This has previously been advocated (Blondeau-Patissier et al. 2009) and achieved (Komick et al. 2009) over short spatial scales from estuaries to coastal areas with MODIS data. This has never been done over such large spatial scales as the North Sea due to a lack of IOP data and with MERIS data. We characterized both the spatial and temporal patterns in sIOP using a large data base, and simplified these to three principal clusters. Some empiricism is involved in this approach in the relationship between IOP and biogeochemical concentrations. Even where there is large variability in the spatial and temporal trends in the sIOP (Figure 2, 4, 5), as long as the basis vector of sIOP in the region is well characterised, the retrievals should be accurate, which we proved to be the case with the exception of TSM at concentrations <1 g m^{-3}. The only deviation from these will come from errors in $nL_w(\lambda)$ arising from the atmospheric correction model or low signal to noise ratio. These should be significantly improved in future generation MERIS products.

Rather than using fixed bands, the HYDROPT algorithm uses full spectral dependence from radiative transfer model output and retains full angular dependence of the radiative transfer output (Van der Woerd and Pasterkamp 2008). This is highly advantageous for sensing in coastal waters when swaths from current spectrometers, such as MERIS and MODIS, are large. It also employs a chi square test to indicate which sIOP suite is most accurate on a pixel by pixel basis. This can also be used to give an uncertainty value of the retrieved product on a pixel by pixel basis (Van der Woerd and Pasterkamp 2008), and could be used to indicate the sIOP type or provide IOP maps (van

der Woerd et al. 2004). The HYDROPT algorithm can be implemented quickly and easily using specific-absorption and scattering coefficients from a LUT which tabulates the relationship between remote sensing reflectance and a range of IOP calculated from a forward radiative transfer model. HYDROPT can also be quickly re-calibrated, using an 'external' suite of sIOP, making it simple and easy to transfer to other regions using representative specific-absorption groups. The only limitations are that the vertical distribution of IOP is not accounted for as the method presented is based solely on surface sIOP, which is justified when water column is homogeneous but may incur errors in non-homogenous water bodies.

Similar $a_{ph}^*(442)$ and $a_{CDOM}(442)$ values to those we report for the North Sea are found along the Mid and Southern Atlantic Bights (Nelson et al. 1998), in the Mississippi river plume and US Louisiana coast (D'Sa and Miller 2003) and the Rhode Island coast (Keith et al. 2002). This suggests that HYDROPT could be accurate for these areas and could be easily implemented using an sIOP suite characteristic of each region. The newly parameterized HYDROPT algorithm provides accurate Chla, TSM and a_{CDOM} products for the North Sea and other coastal areas and may prove to be even more accurate with the 3rd reprocessing MERIS data.

5. Conclusions

The high spatial and temporal variation in IOP in coastal waters makes the construction of robust global coastal ocean colour models difficult. In this paper we addressed the question of whether trends in specific-absorption properties alone can be used to develop more accurate ocean colour regional algorithms? *In situ* data were collected from 468

stations sampled over 21 cruises between 1999 and 2003 in the North Sea covering an area of approximately 13 million km^2. There was a marked geographic difference between some parameters: Chla was significantly higher along the Dutch Coast, TSM was highest along the Dutch, Belgium and German coasts and $a_{CDOM}(442)$ was higher in the German Bight and Skagerrak. Cluster analysis on specific-absorption properties classified our study region into three main groups; low a_{ph}^*, high a_{NAP}^* and a_{CDOM} close to the coast, medium a_{ph}^*, a_{NAP}^* and a_{CDOM} over the shelf and high a_{ph}^*, low a_{NAP}^* and a_{CDOM} further offshore.

Based on ~60 independent, co-incident satellite match-up stations, we found that the semi-analytical ocean colour algorithm HYDROPT, parameterized with sIOP data sets derived from the cluster analysis, gave more accurate Chla and $a_{CDOM}(442)$ products and similarly accurate TSM retrievals at values >1 g m^{-3} compared to standard MERIS Case 2 products. These results suggest that careful parameterization of semi-analytical ocean colour algorithms with sufficient sIOP data to be representative of the salient trends in the absorption properties, can significantly improve the accuracy of ocean colour products in coastal waters. These improved HYDROPT products using MERIS data could benefit the ongoing monitoring of phytoplankton in coastal waters under changing anthropogenic and climatic conditions.

Acknowledgements. We thank the captains and crews of *RV Belgica, RRS Discovery, RV Heincke, RRS James Clark Ross, RV Mitra, RV Squila, RV Trygve Braarud, MS Wappen von Hamburg* and *RV Water Guardian* and NEODAAS UK for cruise support. We also thank Alice Chapman of the EA UK for ship time, Reinold Pasterkamp, Jo Høkedal and Rosa Astoreca for sample collection and analyses. We are indebted to Denise

Cummings, Merete Grung and Kirsten Heymann for HPLC analysis. We also thank Dr. Roland Doerffer as part of the REVAMP team. The research was conducted within the EU FP 5 'Regional Validation of MERIS Chlorophyll Products in North Sea Coastal Waters' (contract EVG1-CT-2001-00049) which supported all authors except Dr. Shutler. Dr. Kevin Ruddick was also supported by the Belgian Federal Science Policy Office project BELCOLOUR (SR/00/003), Dr. Sørensen by the Norwegian VAMP (ESA PRODEX no. 14849/00/NL/Sfe(IC)), Drs. van der Woerd, Eleveld & Peters by BSIK Climate Changes Spatial Planning A6 and Drs. Tilstone & Shutler were also supported by NERC Oceans 2025 and COASTCOLOUR.

References

(!!! INVALID CITATION !!!).

Aanesen, R.T., Eilertsen, H.C., & Stabell, O.B. (1998). Light-induced toxic properties of the marine alga Phaeocystis pouchetii towards cod larvae. *Aquatic Toxicology, 40*, 109-121

Aarup, T., Holt, N., & Hojerslev, N.K. (1996). Optical measurements in the North Sea-Baltic Sea transition zone .2. Water mass classification along the Jutland west coast from salinity and spectral irradiance measurements. *Continental Shelf Research, 16*, 1343-1353

Antoine, D., d'Ortenzio, F., Hooker, S.B., Becu, G., Gentili, B., Tailliez, D., & Scott, A.J. (2008). Assessment of uncertainty in the ocean reflectance determined by three satellite ocean color sensors (MERIS, SeaWiFS and MODIS-A) at an offshore site in the Mediterranean Sea (BOUSSOLE project). *Journal of Geophysical Research-Oceans, 113*, C07013, doi:07010.01029/02007JC004472

Antoine, D., Morel, A., Gordon, H.R., Banzon, V.F., & Evans, R.H. (2005). Bridging ocean color observations of the 1980s and 2000s in search of long-term trends. *Journal of Geophysical Research-Oceans, 110*

Astoreca, R., Rousseau, V., & Lancelot, C. (2009). Coloured dissolved organic matter (CDOM) in Southern North Sea waters: Optical characterization and possible origin. *Estuarine Coastal and Shelf Science, 85*, 633-640

Aznay, O., & Santer, R. (2009). MERIS atmospheric correction over coastal waters: validation of the MERIS aerosol models using AERONET. *International Journal of Remote Sensing, 30*, 4663-4684

Babin, M., Morel, A., Fournier-Sicre, V., Fell, F., & Stramski, D. (2003a). Light scattering properties of marine particles in coastal and open ocean waters as related to the particle mass concentration. *Limnology and Oceanography, 48*, 843-859

Babin, M., Stramski, D., Ferrari, G.M., Claustre, H., Bricaud, A., Obolensky, G., & Hoepffner, N. (2003b). Variations in the light absorption coefficients of phytoplankton,

nonalgal particles, and dissolved organic matter in coastal waters around Europe. *Journal of Geophysical Research-Oceans, 108*, C73211, doi:73210.71029/72001JC000882
Babin, M., Stramski, D., Ferrari, G.M., Claustre, H., Bricaud, A., Obolensky, G., & Hoepffner, N. (2003c). Variations in the light absorption coefficients of phytoplankton, nonalgal particles, and dissolved organic matter in coastal waters around Europe. *Journal of Geophysical Research-Oceans, 108*
Blondeau-Patissier, D., Brando, V.E., Oubelkheir, K., Dekker, A.G., Clementson, L.A., & Daniel, P. (2009). Bio-optical variability of the absorption and scattering properties of the Queensland inshore and reef waters, Australia. *Journal of Geophysical Research-Oceans, 114*
Bousquet, P., Ciais, P., Miller, J.B., Dlugokencky, E.J., Hauglustaine, D.A., Prigent, C., Van der Werf, G.R., Peylin, P., Brunke, E.G., Carouge, C., Langenfelds, R.L., Lathiere, J., Papa, F., Ramonet, M., Schmidt, M., Steele, L.P., Tyler, S.C., & White, J. (2006). Contribution of anthropogenic and natural sources to atmospheric methane variability. *Nature, 443*, 439-443
Bowers, D., & Mitchelson-Jacob, E. (1996). Inherent optical properties of the Irish Sea determined from underwater irradiance measurements. *Estuarine Coastal and Shelf Science, 43*, 433-447
Bowers, D.G., & Binding, C.E. (2006). The optical properties of mineral suspended particles: A review and synthesis. *Estuarine Coastal and Shelf Science, 67*, 219-230
Bowers, D.G., Harker, G.E.L., Smith, P.S.D., & Tett, P. (2000). Optical properties of a region of freshwater influence (The Clyde Sea). *Estuarine Coastal and Shelf Science, 50*, 717-726
Bricaud, A., Claustre, H., Ras, J., & Oubelkheir, K. (2004a). Natural variability of phytoplanktonic absorption in oceanic waters: Influence of the size structure of algal populations. *Journal of Geophysical Research-Oceans, 109*, C11010, doi:11010.11029/12004JC002419
Bricaud, A., Claustre, H., Ras, J., & Oubelkheir, K. (2004b). Natural variability of phytoplanktonic absorption in oceanic waters: Influence of the size structure of algal populations. *Journal of Geophysical Research-Oceans, 109*
Campbell, J., Antoine, D., Armstrong, R., Arrigo, K., Balch, W., Barber, R., Behrenfeld, M., Bidigare, R., Bishop, J., Carr, M.E., Esaias, W., Falkowski, P., Hoepffner, N., Iverson, R., Kiefer, D., Lohrenz, S., Marra, J., Morel, A., Ryan, J., Vedernikov, V., Waters, K., Yentsch, C., & Yoder, J. (2002). Comparison of algorithms for estimating ocean primary production from surface chlorophyll, temperature, and irradiance. *Global Biogeochemical Cycles, 16*, art. no.-1035
Carder, K.L., Chen, F.R., Lee, Z.P., Hawes, S.K., & Kamykowski, D. (1999). Semianalytic Moderate-Resolution Imaging Spectrometer algorithms for chlorophyll a and absorption with bio-optical domains based on nitrate-depletion temperatures. *Journal of Geophysical Research-Oceans, 104*, 5403-5421
Clarke, K.R., & Gorley, R.N. (2006). *PRIMER v6: User manual.* . Plymouth Marine Laboratory, Plymouth: Primer-E
Claustre, H., & Maritorena, S. (2003). The many shades of ocean blue. *Science, 302*, 1514-1515

Cota, G.F., Harrison, W.G., Platt, T., Sathyendranath, S., & Stuart, V. (2003). Bio-optical properties of the Labrador Sea. *Journal of Geophysical Research-Oceans, 108*, C73228, doi:73210.71029/72000JC000597
D'Sa, E.J., & Miller, R.L. (2003). Bio-optical properties in waters influenced by the Mississippi River during low flow conditions. *Remote Sensing of Environment, 84*, 538-549
Darecki, M., Weeks, A., Sagan, S., Kowalczuk, P., & Kaczmarek, S. (2003). Optical characteristics of two contrasting Case 2 waters and their influence on remote sensing algorithms. *Continental Shelf Research, 23*, 237-250
Defoin-Platel, M., & Chami, M. (2007). How ambiguous is the inverse problem of ocean color in coastal waters? *Journal of Geophysical Research-Oceans, 112*, 1 - 16
Del Vecchio, R., & Blough, N.V. (2002). Photobleaching of chromophoric dissolved organic matter in natural waters: kinetics and modeling. *Marine Chemistry, 78*, 231-253
Doerffer, R., & Schiller, H. (2007). The MERIS case 2 water algorithm. *International Journal of Remote Sensing, 28*, 517-535
Esaias, W.E., Abbott, M.R., Barton, I., Brown, O.B., Campbell, J.W., Carder, K.L., Clark, D.K., Evans, R.H., Hoge, F.E., Gordon, H.R., Balch, W.M., Letelier, R., & Minnett, P.J. (1998). An overview of MODIS capabilities for ocean science observations. *Ieee Transactions on Geoscience and Remote Sensing, 36*, 1250-1265
Ferrari, G.M., Bo, F.G., & Babin, M. (2003). Geo-chemical and optical characterizations of suspended matter in European coastal waters. *Estuarine Coastal and Shelf Science, 57*, 17-24
Ferrari, G.M., Dowell, M.D., Grossi, S., & Targa, C. (1996). Relationship between the optical properties of chromophoric dissolved organic matter and total concentration of dissolved organic carbon in the southern Baltic Sea region. *Marine Chemistry, 55*, 299-316
Foden, J., Sivyer, D.B., Mills, D.K., & Devlin, M.J. (2008). Spatial and temporal distribution of chromophoric dissolved organic matter (CDOM) fluorescence and its contribution to light attenuation in UK waterbodies. *Estuarine Coastal and Shelf Science, 79*, 707-717
Garver, S.A., & Siegel, D.A. (1997). Inherent optical property inversion of ocean color spectra and its biogeochemical interpretation .1. Time series from the Sargasso Sea. *Journal of Geophysical Research-Oceans, 102*, 18607-18625
Gomez-Chova, L., Camps-Valls, G., Calpe-Maravilla, J., Guanter, L., & Moreno, J. (2007). Cloud-screening algorithm for ENVISAT/MERIS multispectral images. *Ieee Transactions on Geoscience and Remote Sensing, 45*, 4105-4118
Hedges, J.I., Keil, R.G., & Benner, R. (1997). What happens to terrestrial organic matter in the ocean? *Organic Geochemistry, 27*, 195-212
Hojerslev, N.K., Holt, N., & Aarup, T. (1996). Optical measurements in the North Sea-Baltic Sea transition zone .1. On the origin of the deep water in the Kattegat. *Continental Shelf Research, 16*, 1329-1342
Hokedal, J., Aas, E., & Sorensen, K. (2005). Spectral optical and bio-optical relationships in the Oslo Fjord compared with similar results from the Baltic Sea. *International Journal of Remote Sensing, 26*, 371-386
Holligan, P.M., Aarup, T., & Groom, S.B. (1989). The North-Sea - Satellite Color Atlas. *Continental Shelf Research, 9*, 665-765

Hooker, S.B., & Morel, A. (2003). Platform and environmental effects on above-water determinations of water-leaving radiances. *Journal of Atmospheric and Oceanic Technology, 20*, 187-205
IOCCG (2000). Remote sensing of Ocean Colour in Coastal and Other Optically-Complex Waters. . In S. Sathyendranath & V. Stuart (Eds.), *IOCCG report* (pp. 1-137). Canada: Bedford Institute of Oceanography
IOCCG (2006). *Remote Sensing of Inherent Optical Properties: Fundamentals, tests of algorithms and*
774 applications. Dartmouth, Canada: IOCCG
Jeffrey, S.W., Mantoura, R.F.C., & Wright, S.W. (1997). *Phytoplankotn pigments in oceanography*. Paris: UNESCO
Justic, D., Rabalais, N.N., & Turner, R.E. (1996). Effects of climate change on hypoxia in coastal waters: A doubled CO2 scenario for the northern Gulf of Mexico. *Limnology and Oceanography, 41*, 992-1003
Keith, D.J., Yoder, J.A., & Freeman, S.A. (2002). Spatial and temporal distribution of coloured dissolved organic matter (CDOM) in Narragansett Bay, Rhode Island: Implications for phytoplankton in coastal waters. *Estuarine Coastal and Shelf Science, 55*, 705-717
Kishino, M., Takahashi, M., Okami, N., & Ichimura, S. (1985). Estimation of the Spectral Absorption-Coefficients of Phytoplankton in the Sea. *Bulletin of Marine Science, 37*, 634-642
Komick, N.M., Costa, M.P.F., & Gower, J. (2009). Bio-optical algorithm evaluation for MODIS for western Canada coastal waters: An exploratory approach using in situ reflectance. *Remote Sensing of Environment, 113*, 794-804
Lancelot, C., Billen, G., Sournia, A., Weisse, T., Colijn, F., Veldhuis, M.J.W., Davies, A., & Wassman, P. (1987). Phaeocystis Blooms and Nutrient Enrichment in the Continental Coastal Zones of the North-Sea. *Ambio, 16*, 38-46
Lee, Z.P., Carder, K.L., & Arnone, R.A. (2002). Deriving inherent optical properties from water color: a multiband quasi-analytical algorithm for optically deep waters. *Applied Optics, 41*, 5755-5772
Lee, Z.P., & Hu, C.M. (2006). Global distribution of Case-1 waters: An analysis from SeaWiFS measurements. *Remote Sensing of Environment, 101*, 270-276
Loisel, H., Meriaux, X., Berthon, J.F., & Poteau, A. (2007). Investigation of the optical backscattering to scattering ratio of marine particles in relation to their biogeochemical composition in the eastern English Channel and southern North Sea. *Limnology and Oceanography, 52*, 739-752
Maestrini, S.Y., & Graneli, E. (1991). Environmental-Conditions and Ecophysiological Mechanisms Which Led to the 1988 Chrysochromulina-Polylepis Bloom - an Hypothesis. *Oceanologica Acta, 14*, 397-413
Maritorena, S., d'Andon, O.H.F., Mangin, A., & Siegel, D.A. (2010). Merged satellite ocean color data products using a bio-optical model: Characteristics, benefits and issues. *Remote Sensing of Environment, 114*, 1791-1804
Maritorena, S., Siegel, D.A., & Peterson, A.R. (2002). Optimization of a semianalytical ocean color model for global-scale applications. *Applied Optics, 41*, 2705-2714
Martinez-Vicente, V., Land, P.E., Tilstone, G.H., Widdicombe, C., & Fishwick, J.R. (2010). Particulate scattering and backscattering related to water constituents and

seasonal changes in the Western English Channel. *Journal of Plankton Research, 32*, 603-619
Martinez, E., Antoine, D., D'Ortenzio, F., & Gentili, B. (2009). Climate-Driven Basin-Scale Decadal Oscillations of Oceanic Phytoplankton. *Science, 326*, 1253-1256
Mitchell, G., Bricaud, A., Carder, K., Cleveland, J., Ferrari, G., Gould, R., Kahru, M., M., K., Maske, H., Moisan, T., Moore, L., Nelson, N., Phinney, D., Reynolds, R., Sosik, H., Stramski, D., Tassan, S., Trees, C., Weidemann, A., Weiland, J., & Vodacek, A. (2000). Determination of spectral absorption coefficients of particles, dissolved material, and phytoplankton for discrete water samples In Ocean optics protocols for satellite ocean color sensor validation. In G.S. Fargion & J.L. Mueller (Eds.), *NASA Technical Series*. NASA, Goddard Space Flight Center Greenbelt Maryland 125-153
Mobley, C.D. (1999). Estimation of the remote sensing reflectance from above-surface measurements. *Applied Optics, 38*, 7442-7455
Mohr, J.J., & Forsberg, R. (2002). Remote sensing: Searching for new islands in sea ice - Coastlines concealed in polar seas are now more accessible to cartography. *Nature, 416*, 35-35
Morel, A., & Prieur, L. (1977). Analysis of variations in ocean color. *Limnology and Oceanography, 22*, 709-722
Nelson, N.B., Siegel, D.A., & Michaels, A.F. (1998). Seasonal dynamics of colored dissolved material in the Sargasso Sea. *Deep-Sea Research Part I-Oceanographic Research Papers, 45*, 931-957
O'Reilly, J.E., Maritorena, S., Mitchell, B.G., Siegel, D.A., Carder, K.L., Garver, S.A., Kahru, M., & McClain, C. (1998). Ocean color chlorophyll algorithms for SeaWiFS. *Journal of Geophysical Research-Oceans, 103*, 24937-24953
Pegau, W.S., Gray, D., & Zaneveld, J.R.V. (1997). Absorption and attenuation of visible and near-infrared light in water: dependence on temperature and salinity. *Applied Optics, 36*, 6035-6046
Peters, S.W.M., Eleveld, M., Pasterkamp, R., van der Woerd, H., Devolder, M., Jans, S., Park, Y., Ruddick, K., Block, T., Brockmann, C., Doerffer, R., Krasemann, H., Rottgers, R., Schonfeld, W., Jorgensen, P.V., Tilstone, G.H., Martinez-Vicente, V., Moore, G., Sorensen, K., Hokedal, J., Johnsen, T.M., Lomsland, E.R., & Aas, E. (2005). *An atlas of Chlorophyll-a concentrations for the North Sea based on MERIS imagery of 2003.* Amsterdam, The Netherlands.: Vrije Universiteit, Amsterdam
Petzold, T.J. (1972). *Volume scattering function for selected ocean waters.* San Diego, California: Scripps Instiution of Oceanography
Prieur, L., & Sathyendranath, S. (1981). An Optical Classification of Coastal and Oceanic Waters Based on the Specific Spectral Absorption Curves of Phytoplankton Pigments, Dissolved Organic-Matter, and Other Particulate Materials. *Limnology and Oceanography, 26*, 671-689
Reid, P.C., Borges, M.D., & Svendsen, E. (2001). A regime shift in the North Sea circa 1988 linked to changes in the North Sea horse mackerel fishery. *Fisheries Research, 50*, 163-171
Sathyendranath, S., Cota, G., Stuart, V., Maass, H., & Platt, T. (2001). Remote sensing of phytoplankton pigments: a comparison of empirical and theoretical approaches. *International Journal of Remote Sensing, 22*, 249-273

Schiller, H., & Doerffer, R. (2005). Improved determination of coastal water constituent concentrations from MERIS data. *Ieee Transactions on Geoscience and Remote Sensing, 43*, 1585-1591
Siegel, D.A., Maritorena, S., & Nelson, N.B. (2005a). Independence and interdependencies among global ocean color properties: Reassessing the bio-optical assumption. *Journal of Geophysical Research-Oceans, 110*, C07011
Siegel, D.A., Maritorena, S., Nelson, N.B., Behrenfeld, M.J., & McClain, C.R. (2005b). Colored dissolved organic matter and its influence on the satellite-based characterization of the ocean biosphere. *Geophysical Research Letters, 32*, L20605
Sorensen, K., Aas, E., & Hokedal, J. (2007). Validation of MERIS water products and bio-optical relationships in the Skagerrak. *International Journal of Remote Sensing, 28*, 555-568
Staehr, P.A., Markager, S., & Sand-Jensen, K. (2004). Pigment specific in vivo light absorption of phytoplankton from estuarine, coastal and oceanic waters. *Marine Ecology-Progress Series, 275*, 115-128
Stige, L.C., Ottersen, G., Brander, K., Chan, K.S., & Stenseth, N.C. (2006). Cod and climate: effect of the North Atlantic Oscillation on recruitment in the North Atlantic. *Marine Ecology-Progress Series, 325*, 227-241
Tassan, S., & Ferrari, G.M. (1995). Proposal for the measurement of backward and total scattering by mineral particles suspended in water. *Applied Optics, 34*, 8345-8353
Tassan, S., & Ferrari, G.M. (1998). Measurement of light absorption by aquatic particles retained on filters: determination of the optical pathlength amplification by the 'transmittance-reflectance' method. *Journal of Plankton Research, 20*, 1699-1709
Tilstone, G.H., Moore, G.F., Sorensen, K., Doerffer, R., Rottgers, R., Jorgensen, P.V., Martinez-Vicente, V., & Ruddick, K.G. (2004a). Regional Validation of MERIS Chlorophyll products in North Sea coastal waters: MAVT Inter-calibration report In, *Proceedings of the ENVISAT validation workshop European Space Agency*. Frascatti, Italy, http://envisat.esa.int/workshops/mavt_2003/MAVT-2003_803_REVAMP_Intercal_report_final.pdf European Space Agency
Tilstone, G.H., Moore, G.F., Sorensen, K., Doerffer, R., Rottgers, R., Ruddick, K.G., Jorgensen, P.V., & Pasterkamp, R. (2004b). Regional Validation of MERIS Chlorophyll products in North Sea coastal waters: REVAMP protocols. In, *ENVISAT validation workshop European Space Agency*. Frascatti, Italy, http://envisat.esa.int/workshops/mavt_2003/MAVT-2003_802_REVAMPprotocols3.pdf: European Space Agency
Tilstone, G.H., Smyth, T.J., Gowen, R.J., Martinez-Vicente, V., & Groom, S.B. (2005). Inherent optical properties of the Irish Sea and their effect on satellite primary production algorithms. *Journal of Plankton Research, 27*, 1127-1148
Van der Linde, D. (1998). *Protocol for Total Suspended Matter estimate.*: JRC
van der Woerd, H., & Pasterkamp, R. (2004). Mapping of the North Sea turbid coastal waters using SeaWiFS data. *Canadian Journal of Remote Sensing, 30*, 44-53
Van der Woerd, H.J., & Pasterkamp, R. (2008). HYDROPT: A fast and flexible method to retrieve chlorophyll-a from multispectral satellite observations of optically complex coastal waters. *Remote Sensing of Environment, 112*, 1795-1807

Vantrepotte, V., Brunet, C., Meriaux, X., Lecuyer, E., Vellucci, V., & Santer, R. (2007). Bio-optical properties of coastal waters in the Eastern English Channel. *Estuarine Coastal and Shelf Science, 72*, 201-212
Ward, J.H. (1963). Hierarchical Grouping to Optimize Objective Function. *Journal of the American Statistical Association, 77*, 841-847
WetLabs (2007). ac-9 Protocol In, *Revision L*: WetLabs, USA
Yentsch, C.S., & Phinney, D.A. (1989). A Bridge between Ocean Optics and Microbial Ecology. *Limnology and Oceanography, 34*, 1694-1705
Yunev, O.A., Moncheva, S., & Carstensen, J. (2005). Long-term variability of vertical chlorophyll a and nitrate profiles in the open Black Sea: eutrophication and climate change. *Marine Ecology-Progress Series, 294*, 95-107
Zaneveld, R.V., Kitchen, J.C., & Moore, C. (1994). The Scattering Error Correction of Reflecting-Tube Absorption Meters. *Ocean Optics Xii, 2258*, 44-55
Zibordi, G., Berthon, J.F., Melin, F., D'Alimonte, D., & Kaitala, S. (2009). Validation of satellite ocean color primary products at optically complex coastal sites: Northern Adriatic Sea, Northern Baltic Proper and Gulf of Finland. *Remote Sensing of Environment, 113*, 2574-2591
Zibordi, G., Melin, F., & Berthon, J.F. (2006a). Comparison of SeaWiFS, MODIS and MERIS radiometric products at a coastal site. *Geophysical Research Letters, 33*
Zibordi, G., Strombeck, N., Melin, F., & Berthon, J.F. (2006b). Tower-based radiometric observations at a coastal site in the Baltic Proper. *Estuarine Coastal and Shelf Science, 69*, 649-654

Table 1a. Location and dates of 21 REVAMP cruises. DMI – Danish Meteorological Institute, EA - Environment Agency UK, HZG - Institute for Coastal Research Forschungszentrum Geesthacht, IVM - Institute for Environmental Studies, MUMM – Mathematical modelling unit for the North Sea, NIVA – Norwegian Institute for Water Research, PML – Plymouth Marine Laboratory, UO – University of Oslo.

Laboratory	**Vessel**	**Dates**	**Location**	**No. stations sampled**
DMI	*DMI local boat*	20 June 1998	Danish Coast	6
DMI	*DMI local boat*	14 June, 11 Sept 1999	Danish Coast	20
PML	*RV Discovery*	1 – 14 April 2002	Celtic Sea	12
IVM	*RV Mitra*	8 April 2002	Dutch Coast	4
HZG	*RV Heincke*	24 April – 1 May 2002	German Bight	40
MUMM & PML	*RV Belgica*	3 – 9 May 2002	Celtic Sea	11
NIVA	*RV Trygve Braarud*	7 – 14 May 2002	Skagerrak	7
NIVA	*RV Trygve Braarud*	1 – 5, 24 – 28 June, 1 – 3, 16 – 17, 30 July, 1 – 7, 17, 27 - 28 Aug, 3, 18 Sept 2002.	Skagerrak / Kattegat	35
MUMM & PML	*RV Belgica*	18 – 21 June 2002	Belgium to UK transect	15

EA & PML	*RV Water Guardian*	25 – 26 June 2002	The Wash, Eastern UK coast.	22
HZG	*MS Wappen von Hamburg*	29 – 30 July, 14 – 15 Aug, 3 Sept 2002	German Bight	10
IVM	*RV Mitra*	3 June, 2 Sept 2002	Dutch coast	8
NIVA	*RV Trygve Braarud*	7 – 10, 20 April, 13 – 16, 22 May, 16 – 19 June, 14 July, 24 – 26 Aug 2003	Skagerrak / Kattegat	23
HZG	*RV Heincke*	23 April – 1 May 2003	German Bight	35
MUMM & PML	*RV Belgica*	6 – 8 May 2003	Celtic Sea	5
MUMM & PML	*RV Belgica*	16 – 20 June 2003	Belgium to UK transect	15
PML	*RV James Clark Ross*	1 – 4 August 2003	Celtic Sea	4
HZG	*MS Wappen von Hamburg*	15 July, 5-6 August, 17 Sept 2003	German Bight	23
IVM	*RV Mitra*	23 – 24 April, 8 – 18 July, 10 – 17 July 2003.	Central North Sea	30
PML	*RV Squila*	Weekly sampling, March – Sept 2003	L4, Plymouth Sound, WEC.	32
HZG	*MS Wappen von*	28 July, 3-6 August	German Bight	18

	Hamburg	2004		
TOTAL				**468**

Table 1b. Location and dates of 19 cruises used to collect 61 in situ Chla measurements, 51 of nL_w, 52 TSM and 14 $a_{CDOM}(\lambda)$ measurements used for satellite validation.

Laboratory	**Vessel**	**Dates**	**Location**	**No. stations sampled**
MUMM	*RV Belgica 2003-06*	3 March 2003	Belgium coast	1
MUMM	*RV Belgica 2003-11*	22 - 25 April 2003	Belgium to UK transect	6
MUMM	*RV Belgica 2003-16*	16 – 20 June 2003	Belgium to UK transect	9
MUMM	*RV Belgica 2003-19*	7 - 10 July 2003	Belgium coast	2
MUMM	*RV Belgica B04_10B*	3 – 11 May 2004	Belgium coast	2
MUMM	*RV Belgica B04_16*	12 – 16 July 2004	Belgium coast	3
MUMM	*RV Belgica B05_10*	25 – 29 April 2005	Belgium to UK transect	4
MUMM	*RV Belgica*	3 – 8 June 2005	Belgium to UK	2

	B05_13		transect	
MUMM	*RV Belgica*	27 June – 1 July 2005	Belgium to UK	2
	B05_16		transect	
MUMM	*RV Belgica*	12 – 15 Sept 2005	Belgium coast	1
	B05_21			
MUMM	*RV Belgica*	18 – 21 April 2006	Belgium coast	2
	B06_08			
MUMM	*RV Belgica*	18-21 Sept 2006	Belgium to UK	9
	B06_19		transect	
MUMM	*RV Zeeleeuw*	27 June 2003	Belgium coast	1
	2003_440			
MUMM	*RV Zeeleeuw*	27 June 2004	Belgium coast	1
	2004_450			
MUMM	*RV Zeeleeuw*	18 – 19 July 2005	Belgium coast	2
	2005_374			
MUMM &	*RV Zeeleeuw*	29 June – 3 July 2006	Belgium coast	4
PML	*2006_450*			
PML	*RV James Clark*	4 August 2003	Celtic Sea	1
	Ross			
HZG	*MS Wappen von*	23 April, 16 July, 6	German Bight	8
	Hamburg	August 2003		
IVM	*RV Mitra*	14 July 2003.	Central North Sea	1
TOTAL				**61**

Table 2. Performance indices for relative errors in MERIS products compared with *in situ* nL_w, Chla, TSM, $a_{CDOM}(442)$ and $a_{dg}(442)$.

		N	RPD	APD	M	S	RMS	F_{med}	F_{max}	F_{min}
MERIS	412	51	49 (120)	69 (63)	-0.23	0.18	0.30 (0.04)	0.59	0.88	0.39
nL_w	442	51	65 (-2)	64(143)	-0.27	0.16	0.31 (0.06)	0.54	0.77	0.38
	490	51	66 (163)	65(217)	-0.37	0.20	0.42 (0.08)	0.43	0.68	0.27
	560	51	9 (-5)	24 (17)	0.03	0.08	0.09 (0.11)	1.06	1.28	0.88
	665	51	29 (-7)	64 (16)	0.02	0.06	0.08 (0.06)	1.06	1.22	0.91
MERIS	Chla	61	34 **(8)**	56 (40)	-0.06	0.25	4.74 (0.26)	**0.88**	1.55	0.50
Case 2	a_{dg}	14	136(-40)	155(13)	-0.24	0.51	0.44 (0.58)	0.58	**1.87**	0.18
	TSM	52	**70 (22)**	**85 (33)**	-0.22	**0.24**	8.77 **(0.33)**	0.61	**1.07**	**0.35**
HYDR	Chla	61	**29** (13)	**36 (9)**	**-0.08**	**0.15**	**3.43 (0.17)**	0.82	**1.17**	**0.58**
OPT	a_{CDOM}	14	**-8 (-28)**	**31 (19)**	**0.11**	**0.28**	**0.37 (0.31)**	**1.29**	2.45	**0.68**
sIOP	TSM	52	90 (-62)	98 (50)	**-0.14**	0.31	**7.49** (0.34)	**0.72**	1.46	**0.35**

Columns are the relative percentage difference (RPD), absolute percentage difference (APD) mean (M), standard deviation (S), and root mean square (RMS) of the difference error. The geometric mean and one-sigma range of the ratio ($F = Value_{alg}/Value_{meas}$) are given by F_{med}, F_{min}, and F_{max}, respectively; values closer to 1 are more accurate. RPD, APD and RMS values in brackets are values on log data. The algorithm with the highest precision is highlighted in **bold**. nL_w RMS is mW cm^{-2} μm^{-1} sr^{-1}, Chla RMS is mg m^{-3}, TSM is g m^{-3} and a_{CDOM} and a_{dg} are in m^{-1}.

Table 3. Comparison of range and mean ± standard deviation in a_{ph}, a_{NAP}, a_{CDOM}, a_{ph}*, a_{NAP}* and b_p* from our data with other studies in the North Sea and surrounding environments.

Reference	Location	N	Range	Mean ± SD	λ(nm)
a_{ph} (m^{-1})					
Babin et al. [2003a]	North Sea	96	0.015-0.40	0.15	443
Vantrepotte et al. [2007]	English Channel	272	0.036-0.272	0.17	440
Bricaud et al. [2004]	North Atlantic	281	0.02-0.15	Nd	440
Tilstone et al. [2005]	Irish Sea	30	0.014-0.558	0.079±0.141	442
This study	**North Sea**	**413**	**0.007-0.969**	**0.161±0.006**	**442**
a_{ph}* (m^2 mg $Chla^{-1}$)					
Babin et al. [2003a]	North Sea	96	0.008-0.10	0.008	443
Vantrepotte et al. [2007]	English Channel	272	0.015-0.05	0.025	440
Bricaud et al. [2004]	North Atlantic	281	0.044-0.092	Nd	440
Tilstone et al. [2005]	Irish Sea	30	0.02-0.09	0.045±0.006	442
Staer et al. [2004]	Danish Coast	244	0.03-0.06	0.042	442
This study	**North Sea**	**413**	**0.006-0.163**	**0.044±0.039**	**442**
a_{CDOM} (m^{-1})					
Babin et al. [2003a]	North Sea	96	0.04-0.30	nd	443
Vantrepotte et al. [2007]	English Channel	169	0.007-0.65	0.30±0.07	442
Warnock et al. [1999]	North Sea	293	0.066-0.21	nd	442
Bowers et al. (2000)	NW UK coast	25	0.089-1.57	0.378	440
Foden, et al.(2008)	UK coast	585	0.004-0.48	0.031	442
Tilstone et al. [2005]	Irish Sea	30	0.009-0.957	0.376±0.039	442
Darecki et al. (2003)	Baltic Sea	51	0.015-1.7	nd	440
Stedmon et al. [2000]	Skagerrak	586	0.03-1.08	0.56±0.16	442
Sørensen et al. [2007]	Skagerrak	91	0.2-2	0.62	442
Højerslev & Aas [2001]	Skagerrak	1305	nd	0.74±0.16	442
Kowalczuk et al. [1999]	Baltic Sea	888	0.1-1.44	0.37±0.19	442
Astoreca et al. [2009]	Belgium Coast	210	0.20-1.31	nd	442
This study	**North Sea**	**384**	**0.020-2.164**	**0.348±0.013**	**442**
a_{NAP} (m^{-1})					
Babin et al. [2003a]	North Sea	96	0.02-1.00	nd	443
Ferrari et al. (2003)	European coast	60	0.06-0.36	0.12	442
Vantrepotte et al. [2007]	English Channel	272	0.02-0.08	0.047±0.034	440
Tilstone et al. [2005]	Irish Sea	30	0.02-0.08	0.034±0.024	442
Darecki et al. [2003]	Baltic Sea	51	0.01-0.7	nd	440
This study	**North Sea**	**413**	**0.002-2.00**	**0.125±0.010**	**442**
a_{NAP}* (m^2 g TSM^{-1})					
Ferrari et al. (2003)	European coast	60	0.06-0.12	nd	442
This study	**North Sea**	**367**	**0.001-0.159**	**0.025±0.021**	**442**
b_p (m^{-1})					
Bowers & Binding [2006]	Irish Sea	200	0.04-6.32	1.22	555
Martinez-V et al. [2010]	English Channel	99	0.125-1.76	0.555±0.272	532
This study	**North Sea**	**177**	**0.115-3.84**	**0.959±0.739**	**560**
b_p* (m^2 g TSM^{-1})					
Babin et al. [2003a]	North Sea	56	nd	0.54±1.6	555
Bowers & Binding [2006]	Irish Sea	200	nd	0.22±0.02	555
Martinez-V et al. [2010]	English Channel	99	0.177-0.735	0.366±0.30	532

This study	**North Sea**	**177**	**0.030-2.018**	**0.469±0.313**	**560**

Figure Legends

Figure 1. (A) Location of 468 stations sampled from 1998-2003 for the determination of biogeochemical concentrations and absorption properties. The stations are partitioned into 10 geographic regions; dark green circles, Skagerrak; pink, West Jutland; purple, NW North Sea; orange, SE North Sea; red, German Bight; cyanin, East Anglia UK coast; yellow, Dutch coast; brown, Belgium coast; light green, Celtic Sea; blue, Western English Channel. (B) Location of 61 stations sampled from 2003-2006 for satellite accuracy assessment.

Figure 2. Box plots of (A) Chla, (B) $a_{ph}(442)$, (C) $a_{ph}^*(442)$, (D) $a_{CDOM}(442)$, (E) TSM, (F) $a_{NAP}(442)$, (G) $a_{NAP}^*(442)$, (H) $b_p^*(560)$ for the 10 geographic regions given in Figure 1. The boundary of the box closest to zero indicates the 25th percentile, the solid line within the box is the median, the dashed line is the mean and the boundary of the box farthest from zero indicates the 75th percentile. The error bars above and below the box indicate the 90th and 10th percentiles and the points beyond the error bars are outliers.

Figure 3. Scatterplots of (A) $a_{ph}(442)$ as a function of Chla; solid line regression from our data, dotted line Bricaud et al. (2004) regression, (B) $a_{NAP}(442)$ as a function of TSM; solid line regression from our data, dotted line Babin et al. (2003) regression. Symbols as in Figure 1.

Figure 4. Ternary plot showing the relative contribution of (A) $a_{ph}(442)$, $a_{NAP}(442)$ and $a_{CDOM}(442)$ to total absorption in the North Sea. The different coloured Symbols represent the different geographic regions illustrated in Figure 1. (B) The distribution of

the main groups optical types in the North Sea given in (A) shown in the inset as a_{ph} (green circles), a_{NAP} (red circle), a_{CDOM} (yellow circles), a_{ph}-a_{CDOM} (light blue), a_{CDOM}-a_{NAP} (mauve), a_{ph}-a_{CDOM}- a_{NAP} (dark blue). (C) Geographic distribution of main groupings from cluster analysis on $a_{ph}^*(442)$, $a_{NAP}^*(442)$ and $a_{CDOM}(442)$.

Figure 5. Ternary plots showing the temporal change in $a_{ph}(442)$, $a_{NAP}(442)$ and $a_{CDOM}(442)$ during (A) April-May, (B) June-July, (C) August-September, (D) October-March. Symbols as in Figure 1.

Figure 6. Relationship between salinity and (a.) $a_{CDOM}(442)$ and (b.) $a_{NAP}(442)$ with the absorption types shown in Figure 4b. In (a.) and (b.) solid line is regression for a_{NAP}-a_{CDOM} and a_{NAP}-a_{ph}-a_{CDOM} type waters and dashed line is for a_{CDOM} and a_{ph}-a_{CDOM} type waters. Relationship between salinity and (c.) $a_{CDOM}(442)$ and (d.) $a_{NAP}^*(442)$ with the sIOP cluster groups shown in Figure 4c. In (c.) and (d.) solid line is regression for cluster 2 sIOP type and dashed line is for cluster 3 sIOP type.

Figure 7. Range and median (thick line in each plot) of $a_{ph}^*(\lambda)$, $a_{NAP}^*(\lambda)$, $a_{CDOM}(\lambda$ normalized to 442) and $b_p^*(\lambda)$ for Cluster 1, 2 and 3, used to parameterize HYDROPT. For $b_p^*(\lambda)$ Cluster 1, the median is from the original reference value given in van der Woerd and Pasterkamp (2008).

Figure 8. Comparison of *in situ* nL_w with MERIS nL_w for (A) 442, (B) 560 and (C) 665 nm. Solid line is 1:1. The regression equation is given in the inset.

Figure 9. Comparison of *in situ* and satellite derived (A) MERIS Algal Pigment 2 Chla, (B) HYDROPT sIOP Chla, (C) MERIS TSM (D) HYDROPT sIOP TSM, (E) MERIS $a_{dg}(442)$ and (F) HYDROPT sIOP $a_{CDOM}(442)$. Faint dotted lines are the 1:1 line, upper and lower 20% quartiles. In (B), (D) and (F) green circles are Cluster 1, yellow circles are Cluster 2 and red circles are Cluster 3. The regression equation is given in the inset.

Figure 10. Ocean colour maps of (A) MERIS Chla Algal Pigment 2, (B) HYDROPT sIOP Chla, (C) MERIS TSM, (D) HYDROPT sIOP TSM, (E) MERIS $a_{dg}(442)$ and (F) HYDROPT sIOP $a_{CDOM}(442)$ for 22 April 2003.

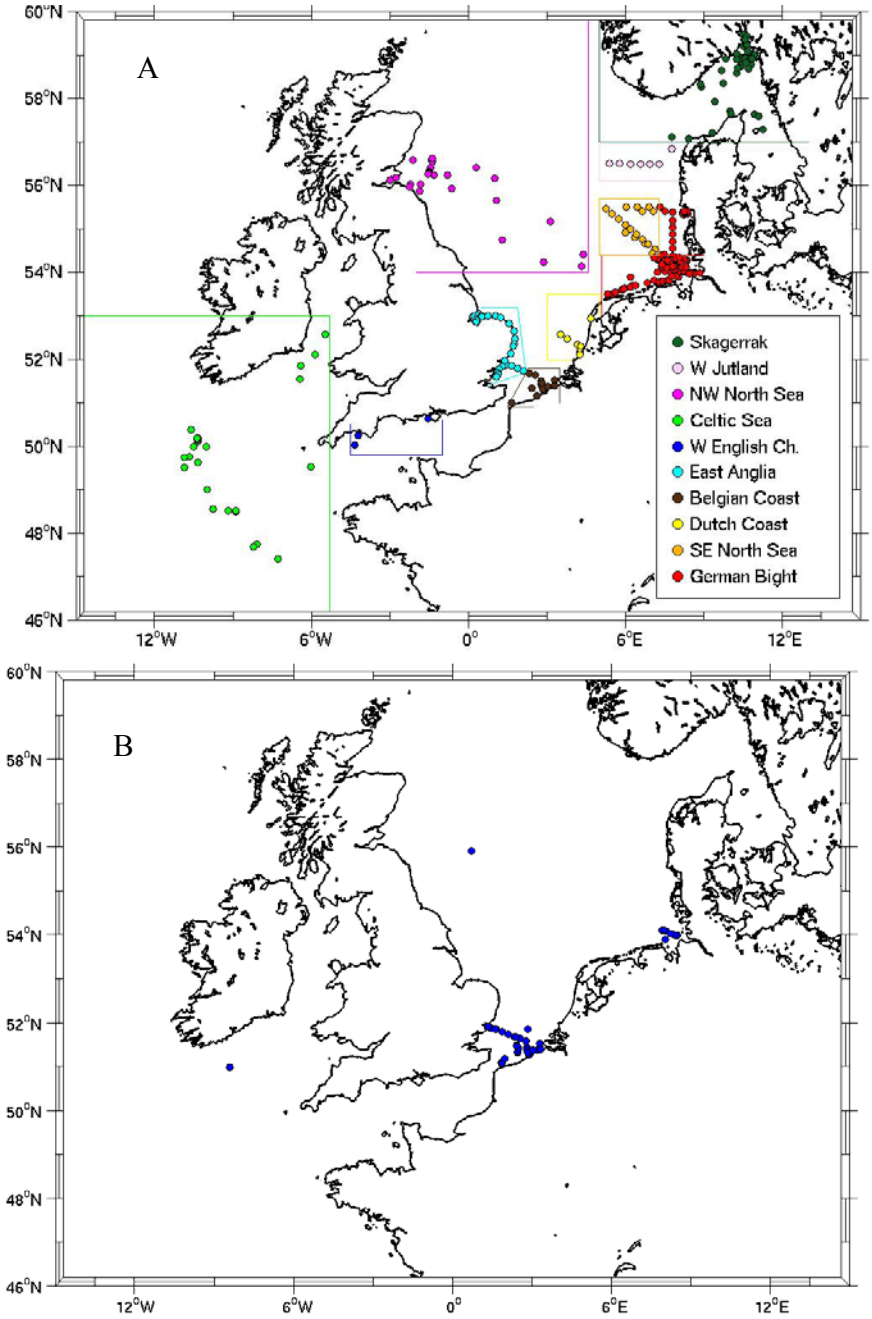

Figure 1. (A) Location of 468 stations sampled from 1998-2003 for the determination of biogeochemical concentrations and absorption properties. The stations are partitioned into 10 geographic regions; dark green circles, Skagerrak; pink, West Jutland; purple, NW North Sea; orange, SE North Sea; red, German Bight; cyanin, East Anglia UK coast; yellow, Dutch coast; brown, Belgium coast; light green, Celtic Sea; blue, Western English Channel. (B) Location of 61 stations sampled from 2003-2006 for satellite accuracy assessment.

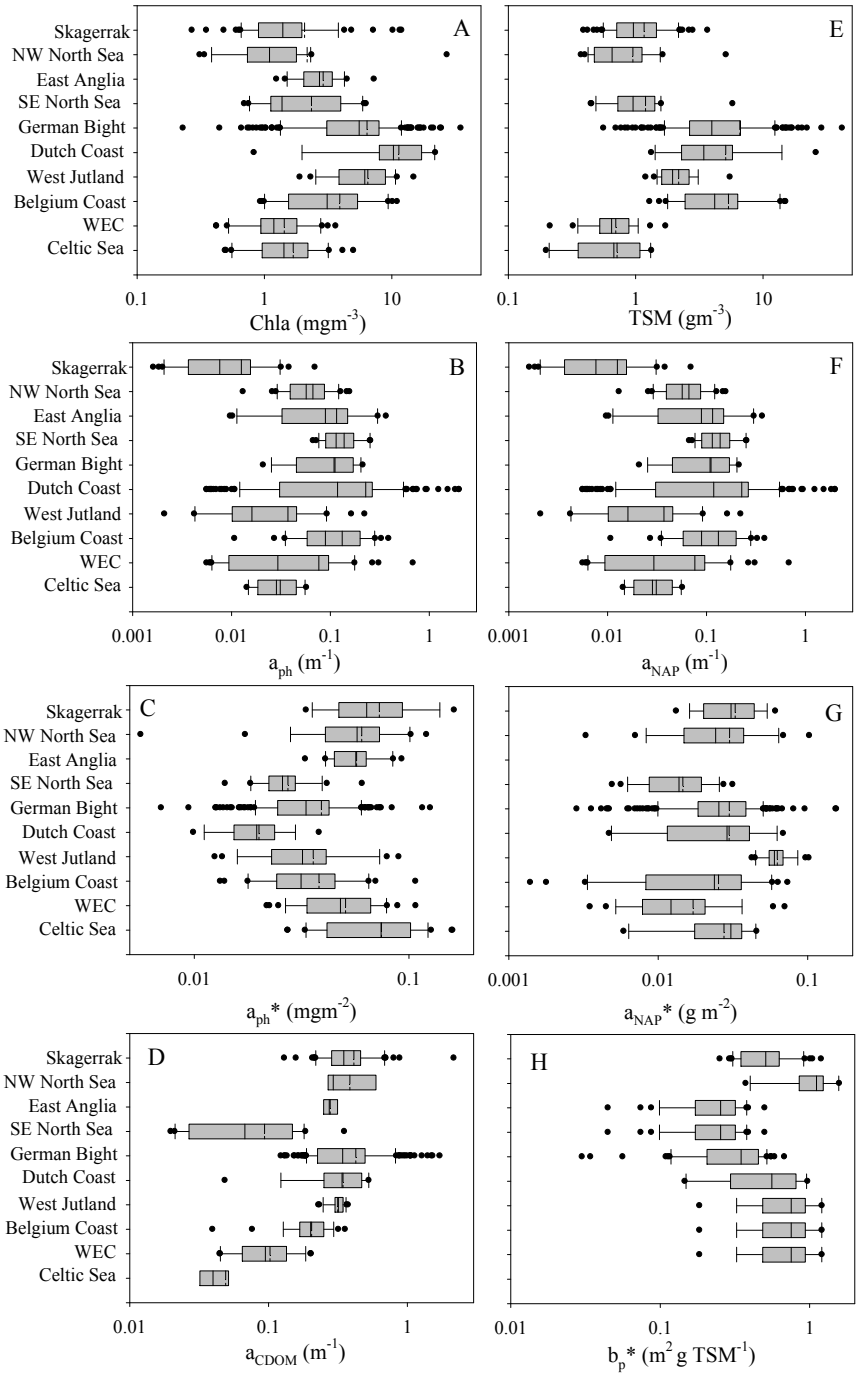

Figure 2. Box plots of (A) Chla, (B) $a_{ph}(442)$, (C) $a_{ph}^*(442)$, (D) $a_{CDOM}(442)$, (E) TSM, (F) $a_{NAP}(442)$, (G) $a_{NAP}^*(442)$, (H) $b_p^*(560)$ for the 10 geographic regions given in Figure 1. The boundary of the box closest to zero indicates the 25th percentile, the solid line within the box is the median, the dashed line is the mean and the boundary of the box farthest from zero indicates the 75th percentile. The error bars above and below the box indicate the 90th and 10th percentiles and the points beyond the error bars are outliers.

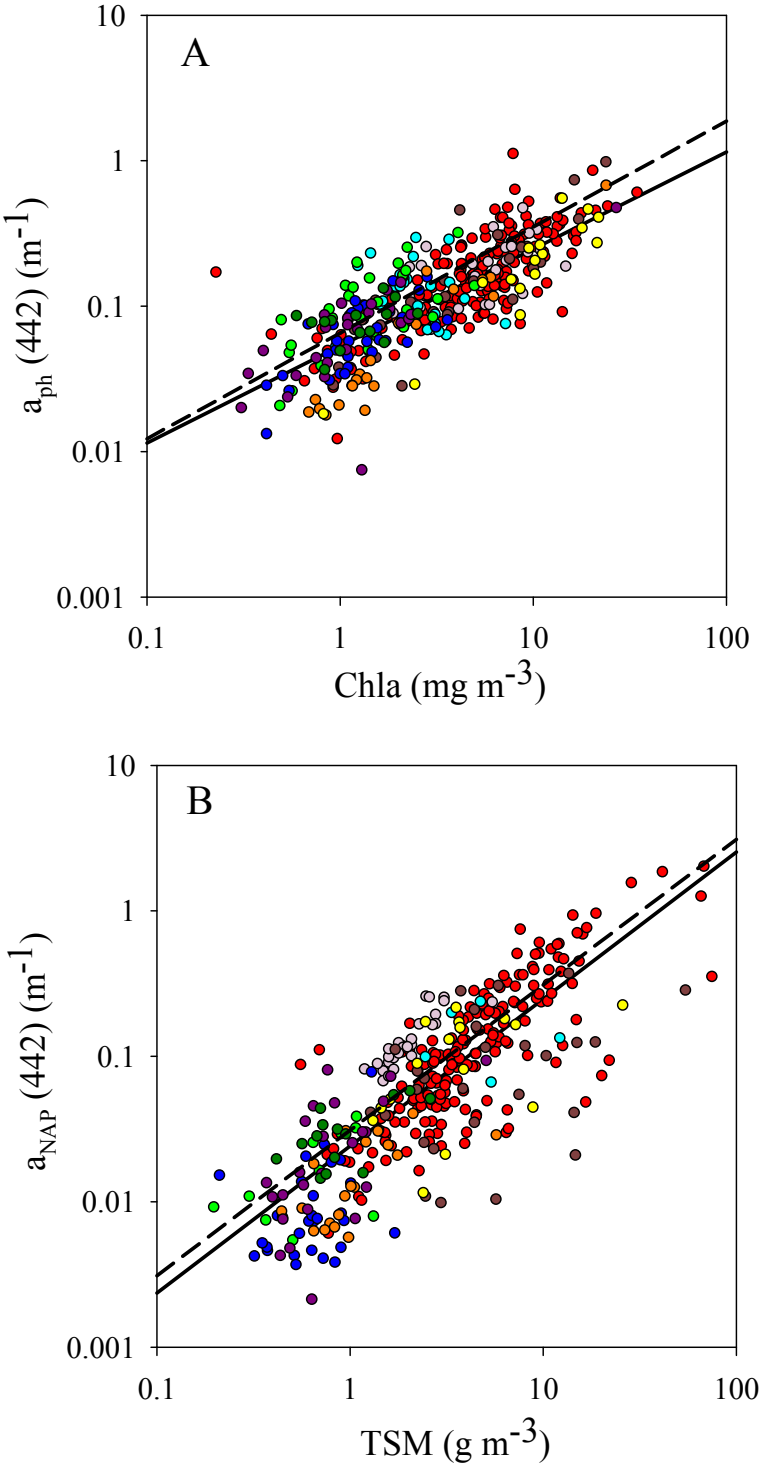

Figure 3. Scatterplots of (A) $a_{ph}(442)$ as a function of Chla; solid line regression from our data, dotted line Bricaud et al. (2004) regression, (B) $a_{NAP}(442)$ as a function of TSM; solid line regression from our data, dotted line Babin et al. (2003) regression. Symbols as in Figure 1.

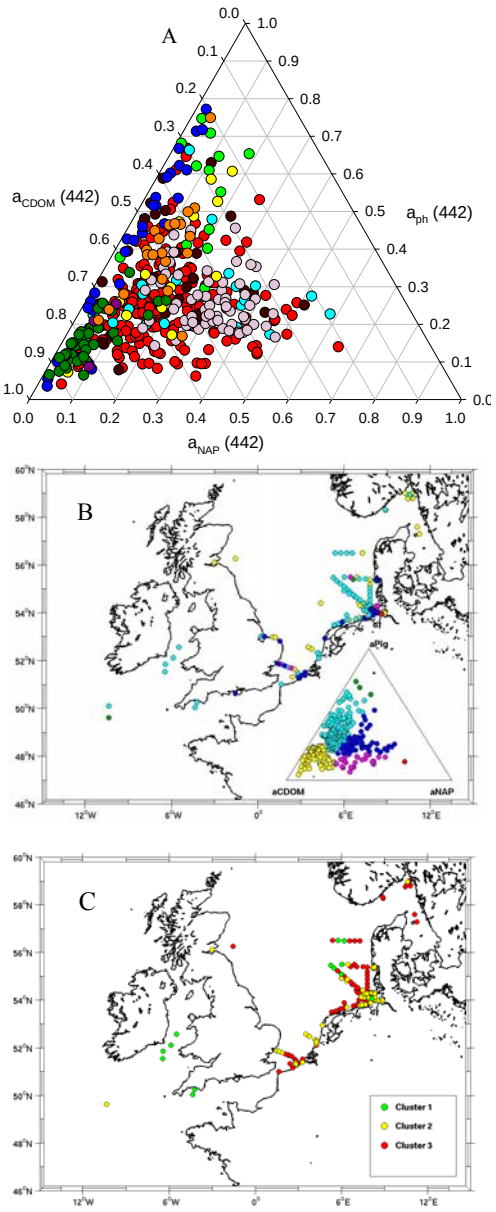

Figure 4. Ternary plot showing the relative contribution of (A) $a_{ph}(442)$, $a_{NAP}(442)$ and $a_{CDOM}(442)$ to total absorption in the North Sea. The different coloured symbols represent the different geographic regions illustrated in Figure 1. (B) The distribution of the main groups optical types in the North Sea given in (A) shown in the inset as a_{ph} (green circles), a_{NAP} (red circle), a_{CDOM} (yellow circles), a_{ph}-a_{CDOM} (light blue), a_{CDOM}- a_{NAP} (mauve), a_{ph}-a_{CDOM}- a_{NAP} (dark blue). (C) Geographic distribution of main groupings from cluster analysis on a_{ph}*(442), a_{NAP}*(442) and $a_{CDOM}(442)$.

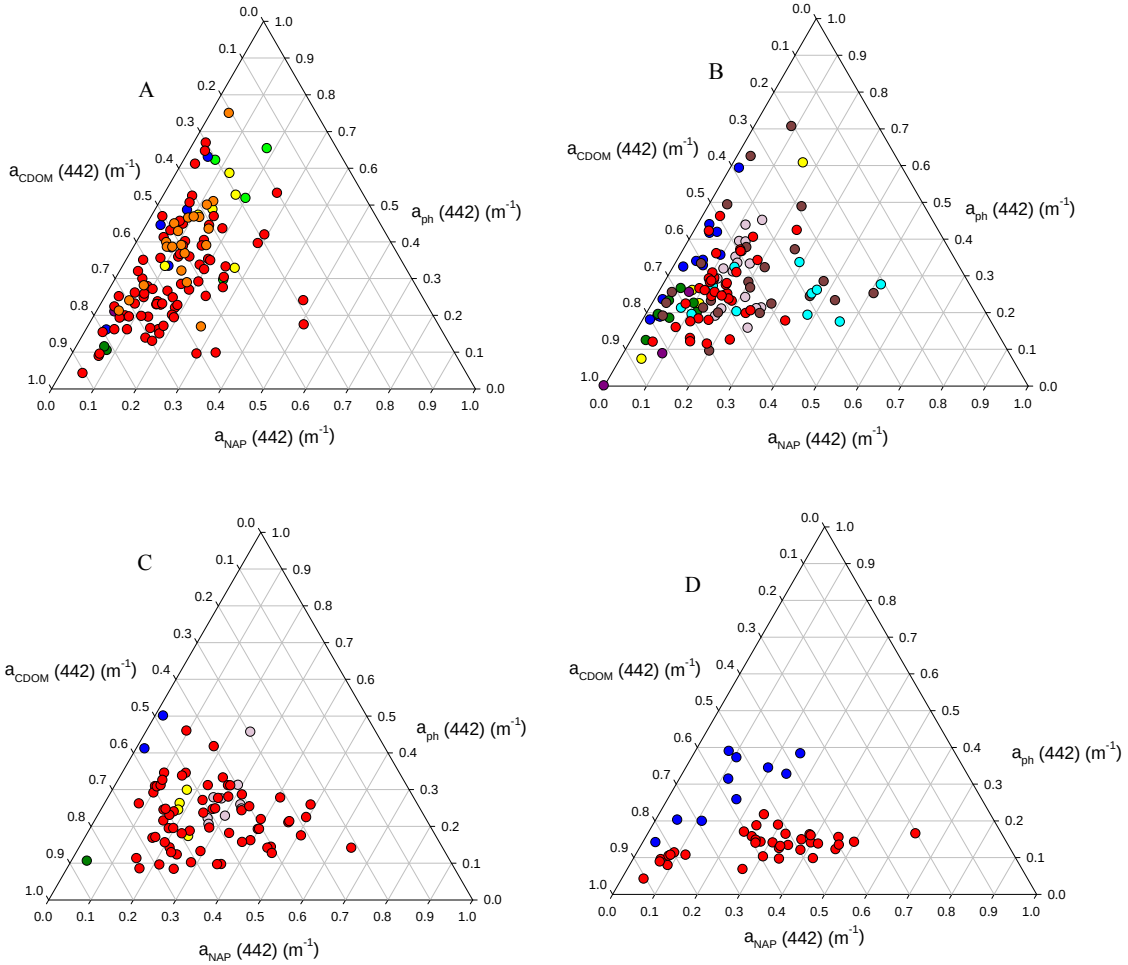

Figure 5. Ternary plots showing the temporal change in $a_{ph}(442)$, $a_{NAP}(442)$ and $a_{CDOM}(442)$ during (A) April-May, (B) June-July, (C) August-September, (D) October-March. Symbols as in Figure 1.

.

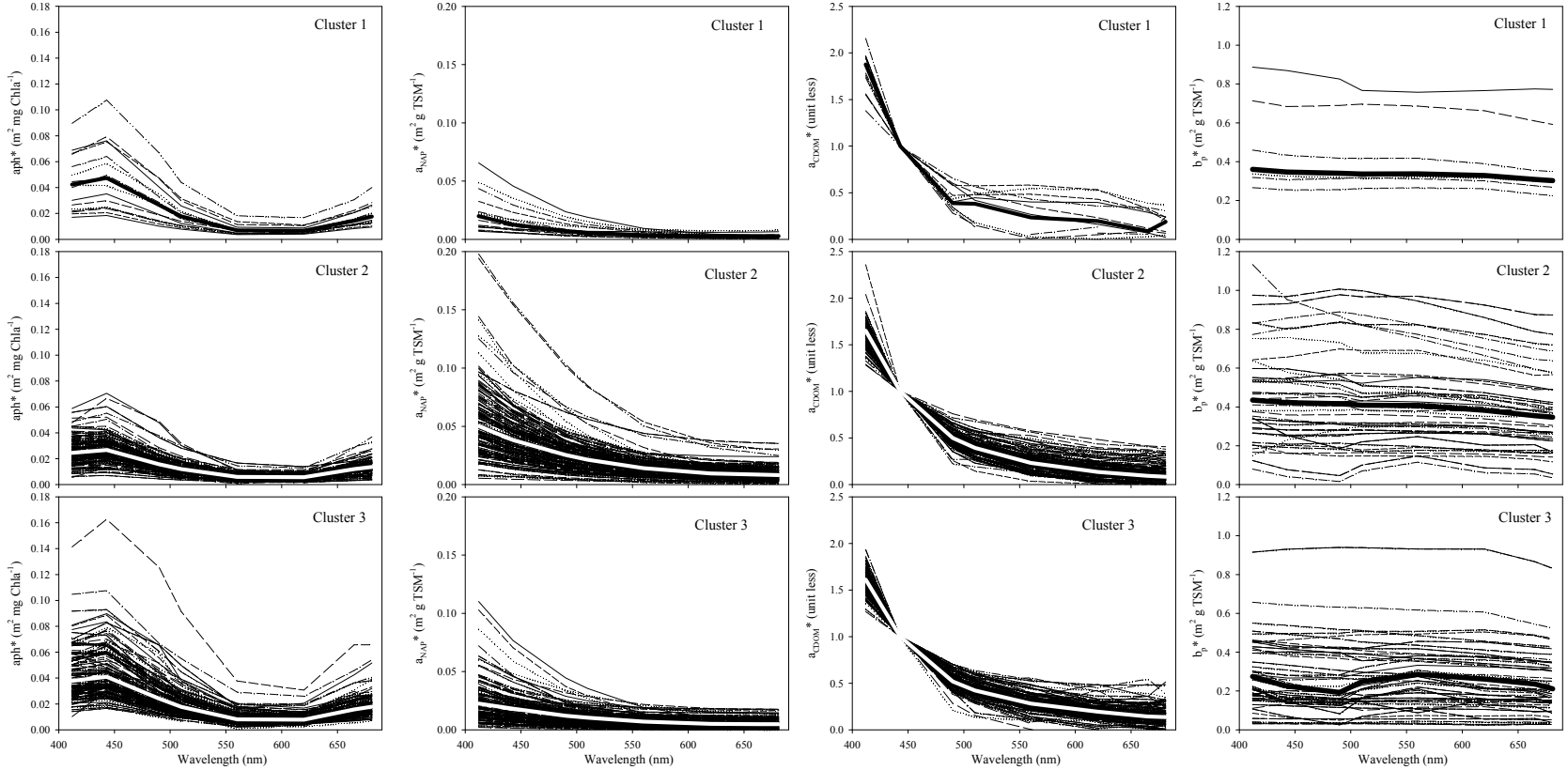

Figure 6. Range and median (thick line in each plot) of $a_{ph}^*(\lambda)$, $a_{NAP}^*(\lambda)$, $a_{CDOM}(\lambda$ normalized to 442) and $b_p^*(\lambda)$ for Cluster 1, 2 and 3, used to parameterize HYDROPT. For $b_p^*(\lambda)$ Cluster 1, the median is from the original reference value given in Van der Woerd and Pasterkamp (2008).

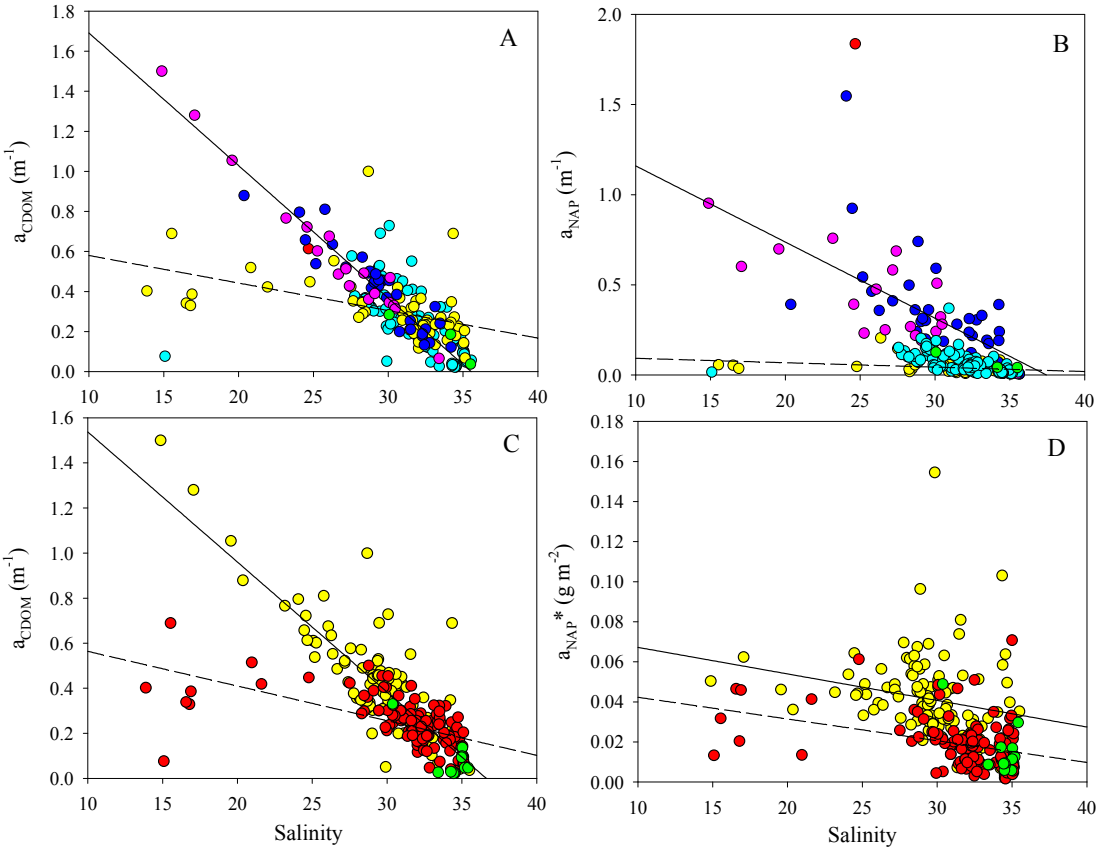

Figure 7. Relationship between salinity and (a.) $a_{CDOM}(442)$ and (b.) $a_{NAP}(442)$ with the absorption types shown in Figure 4b. In (a.) and (b.) solid line is regression for a_{NAP}-a_{CDOM} and a_{NAP}-a_{ph}-a_{CDOM} type waters and dashed line is for a_{CDOM} and a_{ph}-a_{CDOM} type waters. Relationship between salinity and (c.) $a_{CDOM}(442)$ and (d.) a_{NAP}*(442) with the sIOP cluster groups shown in Figure 4c. In (c.) and (d.) solid line is regression for cluster 2 sIOP type and dashed line is for cluster 3 sIOP type.

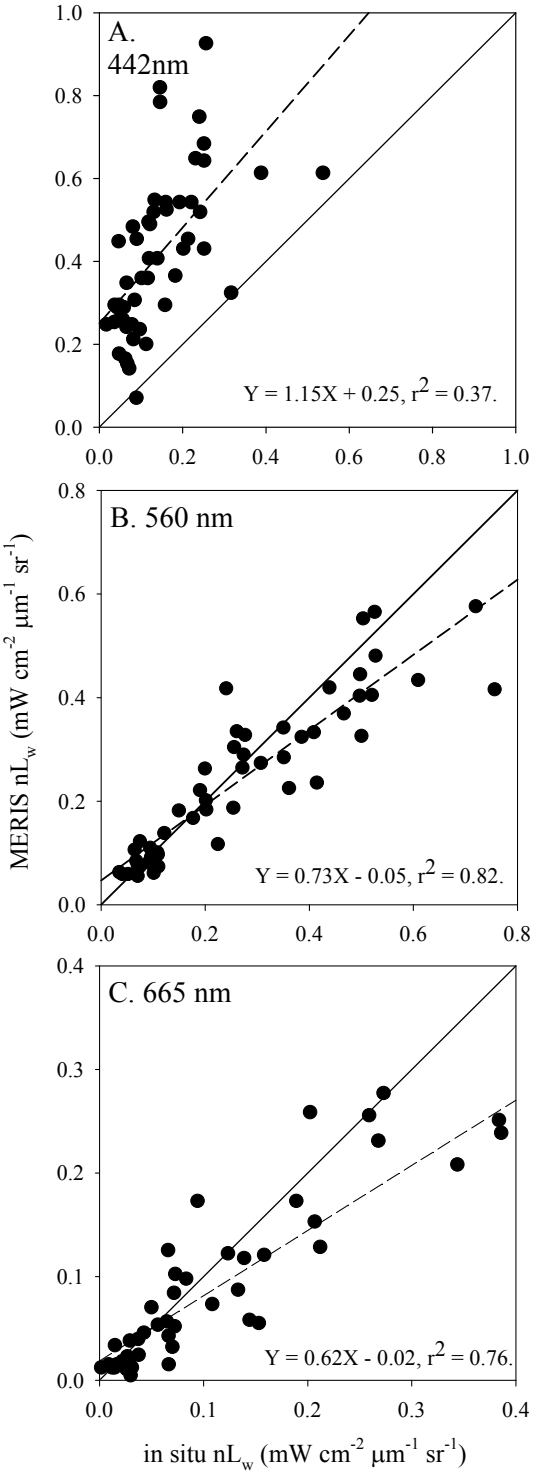

Figure 8. Comparison of *in situ* nL_w with MERIS nL_w for (A) 442, (B) 560 and (C) 665 nm. Solid line is 1:1. The regression equation is given in the inset.

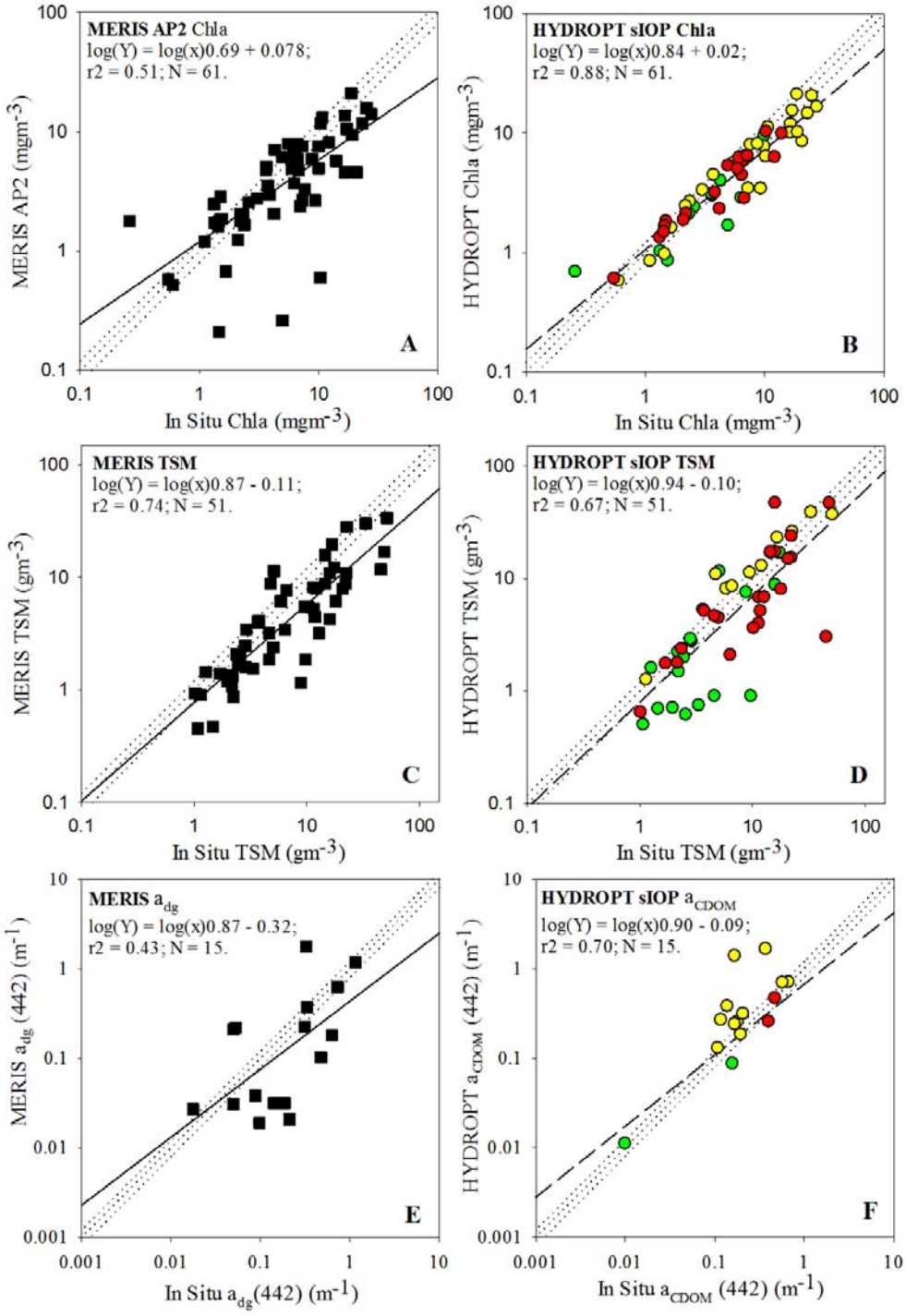

Figure 9. Comparison of *in situ* and satellite derived (A) MERIS Algal Pigment 2 Chla, (B) HYDROPT sIOP Chla, (C) MERIS TSM (D) HYDROPT sIOP TSM, (E) MERIS $a_{dg}(442)$ and (F) HYDROPT sIOP $a_{CDOM}(442)$. Faint dotted lines are the 1:1 line, upper and lower 20% quartiles. In (B), (D) and (F) green circles are Cluster 1, yellow circles are Cluster 2 and red circles are Cluster 3. The regression equation is given in the inset.

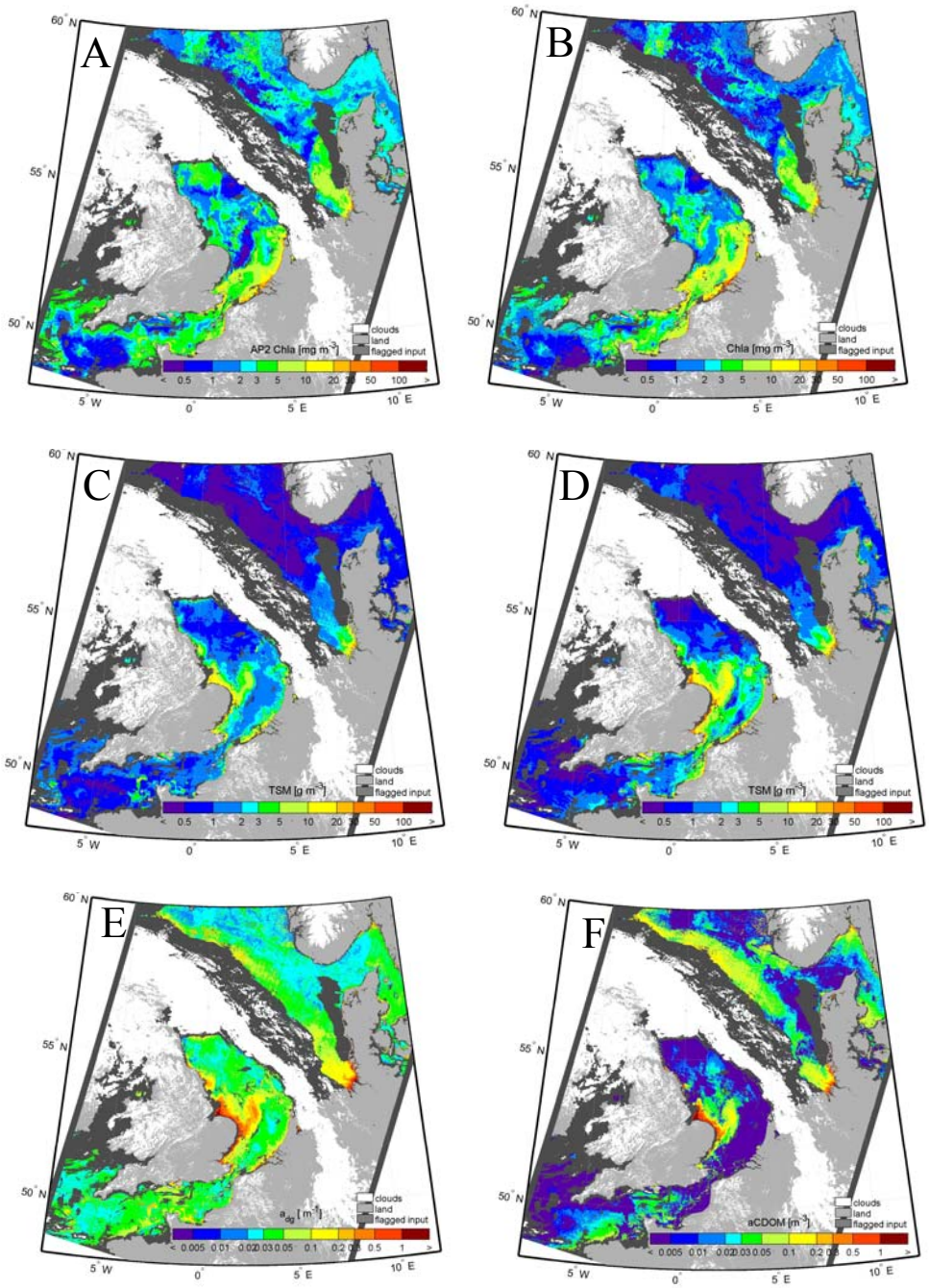

Figure 10. Ocean colour maps of (A) MERIS Chla Algal Pigment 2, (B) HYDROPT sIOP Chla, (C) MERIS TSM, (D) HYDROPT sIOP TSM, (E) MERIS $a_{dg}(442)$ and (F) HYDROPT sIOP $a_{CDOM}(442)$ for 22 April 2003.